ERRATA

Report No. DOT/FAA/TCTT-24/9

Experimental Study of The Characteristics of a Hydrogen Flame from a Small Leak

May 2024

Prepared for

Department of Transportation
Federal Aviation Administration
William J. Hughes Technical Center Atlantic
City International Airport, NJ 08405

Fields 11 and 14 on the Technical Documentation Page have been updated
Replace file tctt24-9.pdf (dated 4/8/2024) with the attached tctt24-9.pdf
(dated 5/23/2024).

Released May 23 2023

1 Attachment: tctt24-9.pdf

Experimental Study of The Characteristics of a Hydrogen Flame from a Small Leak

DOT/FAA/TCTT-24/9

Federal Aviation Administration
William J. Hughes Technical Center
Aviation Research Division
Atlantic City International Airport
New Jersey 08405

April 2024
Technical Thesis

The research described in this report was funded by the FAA as part of its mission to improve aircraft safety. The views and opinions expressed are those of the author alone and do not necessarily represent the views of the FAA. The FAA assumes no liability for the contents or use thereof. The FAA has not edited or modified the contents of the report in any manner.

NOTICE

This document is disseminated under the sponsorship of the U.S. Department of Transportation in the interest of information exchange. The U.S. Government assumes no liability for the contents or use thereof. The U.S. Government does not endorse products or manufacturers. Trade or manufacturers' names appear herein solely because they are considered essential to the objective of this report. The findings and conclusions in this report are those of the author(s) and do not necessarily represent the views of the funding agency. This document does not constitute FAA policy. Consult the FAA sponsoring organization listed on the Technical Documentation page as to its use.

This report is available at the Federal Aviation Administration William J. Hughes Technical Center's Full-Text Technical Reports page: actlibrary.tc.faa.gov in Adobe Acrobat portable document format (PDF).

Technical Report Documentation Page

Form DOT F 1700.7 (8-72) Reproduction of completed page authorized

1. Report No.	2. Government Accession No.	3. Recipient's Catalog No.
DOT/FAA/TCTT-24/9		

4. Title and Subtitle	5. Report Date
Experimental Study of The Characteristics of a Hydrogen Flame from a Small Leak	April 2024
	6. Performing Organization Code

7. Author(s)	8. Performing Organization Report No.
John I. Kurtanidze	

9. Performing Organization Name and Address	10. Work Unit No. (TRAIS)
School of Graduate Studies Rutgers, The State University of New Jersey New Brunswick, NJ	11. Contract or Grant No. 17-G-006

12. Sponsoring Agency Name and Address	13. Type of Report and Period Covered
Federal Aviation Administration William J. Hughes Technical Center Aviation Research Division Atlantic City International Airport Atlantic City NJ 08405	14. Sponsoring Agency Code ANG-E21

15. Supplementary Notes

In partial fulfillment of the requirements for the degree of Master of Science Graduate Program in Mechanical and Aerospace Engineering, Rutgers University.

16. Abstract

With a rising interest in hydrogen-fueled aircraft comes many design and safety concerns. There are many problems to be solved and safety standards and precautions established if aircrafts are going to be equipped with hydrogen. To that end, the objective of this project is to understand the fundamental characteristics of hydrogen flames. More specifically, small hydrogen flames resulting from leaks in diameter of less than 2mm will be studied and their flame characteristics recorded. To simulate leak conditions, a small-scale, horizontal custom hydrogen burner was made with five interchangeable nozzles, each representing a different leak. The nozzles varied in shape between circular and slot orifices, varied in size under 2mm, and the standard leakage flow rate varied was between 1SLPM (Standard Liters Per Minute) and 5SLPM. Nozzle exit-sensor spacing was an additional parameter which was varied between 1in (25mm), 2in (50mm), and 4in (100mm). A water-cooled gardon gauge was utilized to record impinging flame heat flux and K-type thermocouples were used to record cross-sectional flame temperature. Additionally, a flame tracking software was used to estimate the horizontal flame length from the nozzle exit up to the furthest horizontal reach of the flame. Results show that the most influential parameters for leakage flames are the leak size and the flow rate of hydrogen, while the leak shape (whether a crack or a pore) has little influence on the flame characteristics. Generally, increasing standard flow rate (SFR) of hydrogen while keeping leak size constant resulted in an increase in flame heat flux and flame temperature, while increasing the leak size for a given flow resulted in a decrease in flame heat flux and flame temperature. Additionally, reducing the nozzle exit-sensor spacing generally resulted in an increase in flame heat flux while a decrease in flame temperature.

17. Key Words	18. Distribution Statement
	This document is available to the U.S. public through the National Technical Information Service (NTIS), Springfield, Virginia 22161. This document is also available from the Federal Aviation Administration William J. Hughes Technical Center at actlibrary.tc.faa.gov.

19. Security Classif. (of this report)	20. Security Classif. (of this page)	21. No. of Pages	22. Price
Unclassified	Unclassified	66	

EXPERIMENTAL STUDY OF THE CHARACTERISTICS OF A HYDROGEN FLAME FROM A SMALL LEAK

By

JOHN I. KURTANIDZE

A thesis submitted to the

School of Graduate Studies

Rutgers, The State University of New Jersey

In partial fulfillment of the requirements

For the degree of

Master of Science

Graduate Program in Mechanical and Aerospace Engineering

Written under the direction of

Yogesh Jaluria

Francisco Javier Diez

And approved by

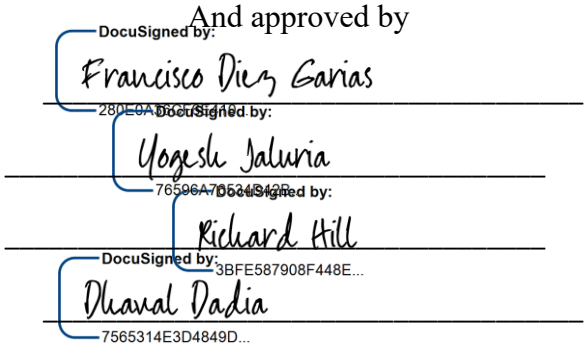

New Brunswick, New Jersey

Winter 2024

ABSTRACT OF THE THESIS

Experimental Study of the Characteristics of a Hydrogen Flame from a Small Leak

by John I. Kurtanidze

Thesis Director:

Yogesh Jaluria
Francisco Javier Diez

With a rising interest in hydrogen-fueled aircraft comes many design and safety concerns. There are many problems to be solved and safety standards and precautions established if aircrafts are going to be equipped with hydrogen. To that end, the objective of this project is to understand the fundamental characteristics of hydrogen flames. More specifically, small hydrogen flames resulting from leaks in diameter of less than 2mm will be studied and their flame characteristics recorded. To simulate leak conditions, a small-scale, horizontal custom hydrogen burner was made with five interchangeable nozzles, each representing a different leak. The nozzles varied in shape between circular and slot orifices, varied in size under 2mm, and the standard leakage flow rate varied was between 1SLPM (Standard Liters Per Minute) and 5SLPM. Nozzle exit-sensor spacing was an additional parameter which was varied between 1in (25mm), 2in (50mm), and 4in (100mm). A water-cooled gardon gauge was utilized to record impinging flame heat flux and K-type thermocouples were used to record cross-sectional flame temperature. Additionally, a flame tracking software was used to estimate the horizontal flame length from the nozzle exit up to the furthest horizontal reach of the flame. Results show that the most influential parameters for leakage flames are the leak size and the flow rate of hydrogen, while the leak shape (whether a crack or a pore) has little influence on the flame characteristics. Generally, increasing standard flow rate (SFR) of hydrogen while

keeping leak size constant resulted in an increase in flame heat flux and flame temperature, while increasing the leak size for a given flow resulted in a decrease in flame heat flux and flame temperature. Additionally, reducing the nozzle exit-sensor spacing generally resulted in an increase in flame heat flux while a decrease in flame temperature.

Acknowledgements

I want to give my thanks to my committee, Professor Francisco Diez Garcia, Professor Yogesh Jaluria, Dhaval Dadia, and Richard Hill, for giving me the opportunity and support to do a project with the Fire Safety Branch of the FAA at the WJHTC facility while completing my Master of Science at Rutgers University. Also, I would like to thank Steven Rehn, Tim Marker, Rob Morrison, and other Fire Safety engineers for their guidance every week for the past year and a half. Their reassurance, support, ideas, and simple conversations helped me gain confidence in my work and in my being in the position I was granted. I want to also thank the technicians who helped me with assembling my experiment and teaching me some manual skills along the way.

Table of Contents

Table of Contents

List of Tables

List of Figures

Section 1: Introduction

1.1 Background on Hydrogen

There is a growing interest in the aviation industry for replacing traditional jet fuel with hydrogen fuel as a means of supplying commercial aircraft propulsion. This concept, however, is not without its challenges. Although hydrogen has been well studied in the past, there is still much unknown in regard to utilizing hydrogen and the safety concerns surrounding it, especially in aviation. Currently, some companies such as ZeroAvia and Universal Hydrogen have been exploring hydrogen-fueled flight for small-scale aircraft and although the promise is to introduce hydrogen-fueled flight in the market within this decade, there is much work to be done to ascertain the safety of bringing hydrogen on-board. There are many risk factors with hydrogen.

Firstly, hydrogen has a high tendency to leak, especially in its gaseous form, due to the tiny hydrogen molecule size, which allows it to naturally permeate through most metals. Extended exposure to hydrogen causes hydrogen embrittlement in many materials which results in the occurrence of cracks and pores in said materials over time [22]. This phenomenon is also known as hydrogen-induced cracking. Hydrogen being the lightest gas in the universe also makes it extremely buoyant and flammable. Hydrogen has a lower flammability limit (LFL) of roughly 4% and upper flammability limit (UFL) of roughly 75% concentration per unit of volume of air [13]. The UFL rises to 94% for a hydrogen-oxygen mixture. In addition, the minimum ignition energy (MIE) for igniting a hydrogen-air mixture is roughly 0.019mJ [13]. This means that an energy source as small as a static charge or a friction spark can set off a hydrogen ignition, therefore hydrogen is

very easy to ignite and very explosive. Thus, the high propensity for leakage coupled with high flammability makes hydrogen leak prevention of outmost priority in any hydrogen vehicle and infrastructure. Therefore, simply equipping an aircraft with a hydrogen tank is an immediate cause for concern. Some studies have been done on the integration of hydrogen onto aircraft and possible design and venting guidelines that may require consideration [20], however, a high-level overview for hydrogen aircraft design is very limited in hydrogen risk factor assessment. To establish proper safety standards, systems, and precautions, a closer look at hydrogen flammability is necessary.

1.2 Literature Review

There has been some work done studying hydrogen flame characteristics at various pressure and flow rate conditions using varying nozzle sizes. Although much of the literature is in relation to hydrogen flammability in context of on-ground hydrogen vehicles, hydrogen infrastructure, and establishing some understanding for safety standards, these studies are still worth considering for aircraft application. For instance, Hentriksen et al. [4] studied high pressure hydrogen jet flames with varying exit-nozzle configurations to measure the flame length. He examined the effects of nozzle geometry on flame length by adjusting upstream and downstream nozzle sizes to create unique flow conditions with gauge pressures at 2-10 MPa and effective nozzle sizes 0.5-4 mm in diameter. He found that the downstream nozzle size had a great influence on the flame length, especially at the lower flow rates. Kobayashi et al. conducted large-scale experiments for high pressure cryo-compressed hydrogen leakage diffusion [6] and ignition and flame analysis [7]. Both studies were in context of on-ground vehicles and the conditions tested were for hydrogen release temperatures of 50-300K, release pressure up to 90MPa from pinhole nozzles of the size between 0.2mm and 1mm at a max flow of 100kg/h. These are extreme conditions, and some findings include that hydrogen leakage flow rate increases in correspondence with a decreased hydrogen supply temperature [6] and consequently, the flame length and blast pressure at ignition for low-temperature hydrogen conditions turn out to be more intense than at higher temperatures due to the hydrogen being denser at lower temperatures, increasing the leakage flow rate and therefore the impact of ignition accidents [7].

On a smaller scale, Panda et al [14] investigated ignition of cryogenic hydrogen release and studied the flame characteristics to generate some critical information to develop safety codes and standards for hydrogen-based infrastructures, such as refueling stations. He measured flame length, radiative heat flux, and max ignition distance at conditions of 37-295K, 2-6bars of absolute pressure, and using nozzle sizes 0.75-1.25mm. He found that maximum ignition distance was greater the lower the temperature of hydrogen, as well as the radiative heat flux being greater at lower temperatures. In addition, he found that the highest heat flux was emitted at location 70-80% up along the flame length and the flame length was shown to directly depend on the speed of the hydrogen release from the nozzle.

Also on a smaller scale, Hecht et al. [3] studied cryogenic hydrogen flames released from crack-shaped nozzles and compared his findings with data of hydrogen flames released from standard circular nozzles. His experiments were under the conditions of hydrogen temperatures between 42-295K, release pressure of 0.5-6 bar (0.05 MPa-0.6 MPa), and nozzle aspect ratios between 2-64. Comparing his data with cryogenic hydrogen released from round nozzles, he found that aspect ratio of the release does not significantly affect the flame characteristics for a given mass flow rate.

Mogi et al. [8] also studied high pressure (0.01-40MPa) hydrogen diffusion flame jets at nozzle exit sizes 0.1-4mm in diameter. He measured the blow-off limits of hydrogen flames as well as the flame size, both length and width. He found that flame size depended both on nozzle size and release pressure and, in the case of slit nozzles, the flame length depended on the length of the shorter side of the slit nozzle. Proust et al. [12] conducted similar experiments for high pressure hydrogen flames and compared his

findings with Mogi. However, Proust focused less on blow-off limits and more on the flame length and heat flux. His findings for flame length were in close agreement with the data provided by Mogi for the various nozzle sizes tested between 1-3mm and gauge pressures up to 90MPa.

Like the work done by Kobayashi et al. [6], there were other studies done about hydrogen leak diffusion, release trajectory, and general hydrogen gas behavior to understand the unburned hydrogen itself. These studies are useful for giving good, baseline understanding of how hydrogen behaves which can give an insight on how hydrogen flames will behave. For instance, Kim et al. [2] did an analytical and experimental study on predicting hydrogen jet and flame trajectories and the effects of buoyancy. The study well distinguishes between buoyancy-controlled and momentum-controlled jets and shows good data on predicting hydrogen jet trajectories based on the Froude Number for jets varying in Reynolds Number up to 2400. In essence, the jets higher in Froude Number (effectively, jets higher in release velocity) would be become more horizontal in their trajectories while the jets lower in Froude Number were mostly dominated by the natural buoyancy property of hydrogen, thus the jet trajectories were more vertical. Shu et al. [16] also studied and provided a prediction model for the motion trajectory of hydrogen leaks in stable, thermally stratified environments. He observed hydrogen leaks released at different angles, leakage velocities, and different thermal stratification of ambient air. The results are complementary with Kim [2]. In addition, Shu illustrated how hydrogen build-up tends to oscillate between the stratification layers and how the amplitude and frequency of these oscillations vary based on the release rate, angle, and the ambient temperature.

Other studies were done on the lower flammability limits (LFL) of hydrogen/air mixtures and how they are affected by various parameters [5]. Results showed that with an increasing ignition energy and initial temperature, the LFL of hydrogen would decrease, while for an increase in initial pressure the LFL of hydrogen would also increase. There were some studies done on accumulation of leaked hydrogen in confined spaces. Hajji et al. [1] conducted a numerical study on how hydrogen may distribute or accumulate in a confined space and varied the roof shape between flat, diamond, and circular and observed the influence of roof shape and leak times on the stratification of hydrogen gas.

1.3 Impinging Jet Flame

Understanding the fundamentals of an impinging jet flame (and a free jet) is also important and relevant to hydrogen flame characterization. Impinging jet flames are well understood and documented. Chander et al. [10] and Dong et al. [11] have done heat transfer analysis and review of impinging jets and give good insight and understanding of what they entail. Wang et al. [9] conducted experiments with a horizontal flame jet impinging on a vertical, flat plate which was covered in thermocouples for acquiring impinging temperature data. Parameters he varied included nozzle diameter 2-4.2mm, standard flow rate 4-22 SLPM, and nozzle exit-plate spacing 0.2-0.4 m. The objective was to understand flame area spread onto an impinging plate and the temperature distribution profile.

To summarize some of the key points discussed by the above authors in their respective papers, the sketch in **Figure 1** was made to illustrate some of the basics of an impinging jet flame, while **Figure 2** and **Figure 3** demonstrate some real-life impinging hydrogen flame jets. Additionally, **Figure 4** demonstrates the invisible nature of hydrogen flames in daylight.

In **Figure 1**, there are three main flame regions identified, the potential core zone, the free jet zone, and the impingement zone. In absence of an impingement wall, there would not be an impingement zone, rather an extended free jet zone, effectively. Some key points regarding these zones in terms of hydrogen flame jets is that a lot of unburned hydrogen can be found in the potential core zone. Due to the flame still being in the early stages of combustion near the exit nozzle, some hydrogen in that region has not been fully burned. Therefore, the flame temperature and heat flux in the potential core zone are

known to be lower than in the other flame regions due to the incomplete combustion. Accordingly, the free jet zone is a region with a lower concentration of unburned hydrogen, therefore having a more complete combustion. Thus, the flame temperature and heat flux in this region is known to be higher. Finally, the impingement zone is where a flame jet impacts a surface and disperses laterally along the surface. Depending on the flow rate, exit-plate spacing, and the size of the nozzle, the surface area impacted by the flame and its dispersion will vary.

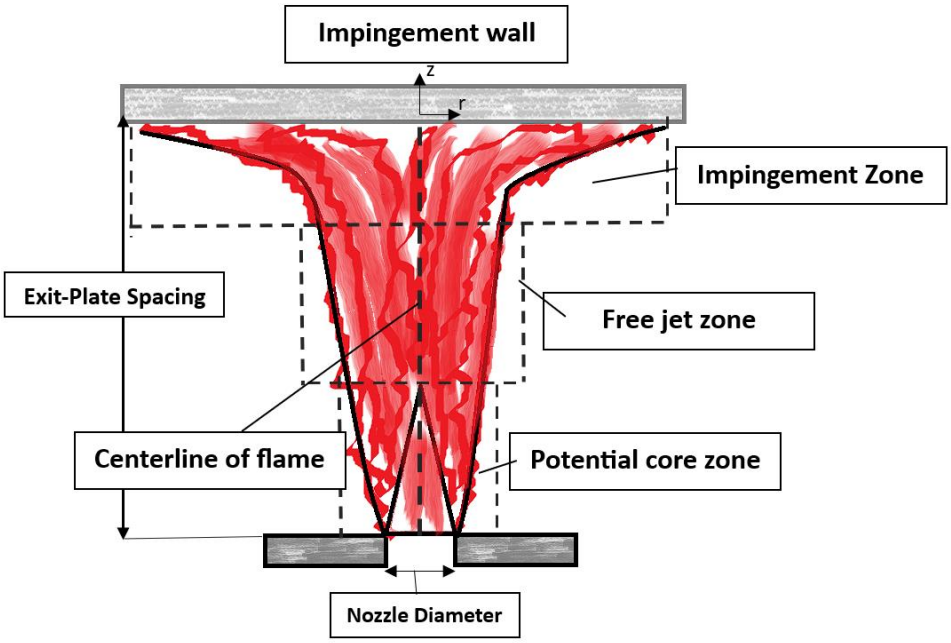

Figure 1: Illustration of an Impinging Flame Jet

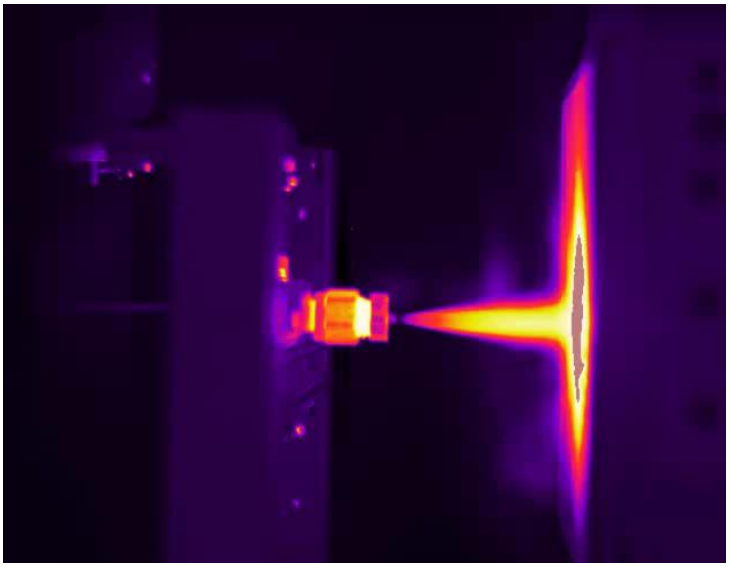

Figure 2: Infrared image of an impinging hydrogen flame jet (side view)

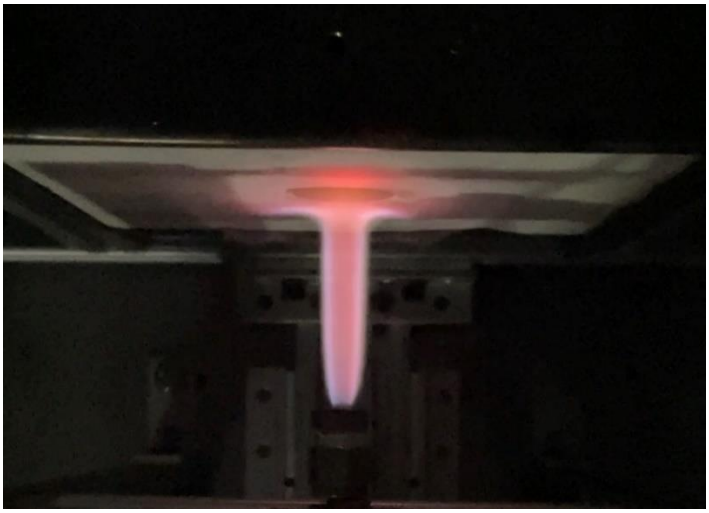

Figure 3: Top view of an impinging hydrogen flame jet (visible in a darkened room)

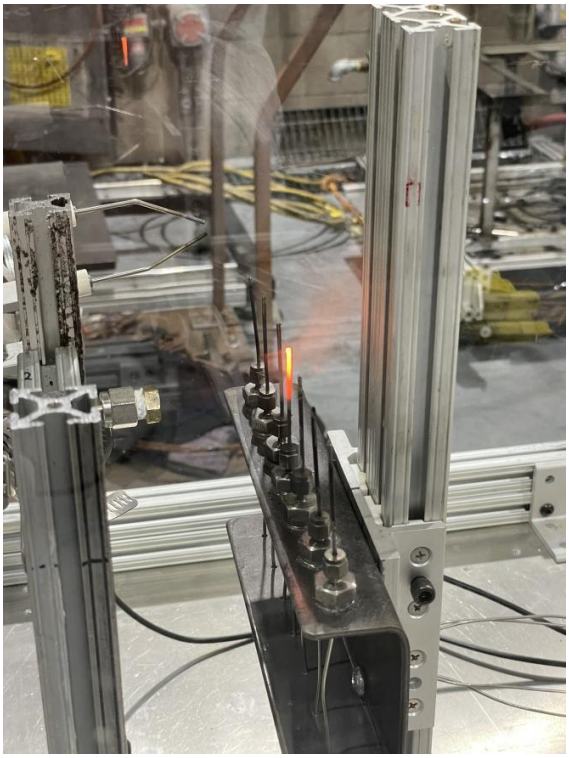

Figure 4: Hydrogen Flame Jet Hitting Thermocouples (flame invisible in a lit room)

1.4 Motivation

Considering the previous work that has been done on hydrogen flames, hydrogen flammability and ignition, dispersion, diffusion, leak release trajectory, and hydrogen buildup and concentration, the current study focuses to do a small-scale study on horizontal hydrogen leakage ignition and characterization of hydrogen flames resulting from leaks of size smaller than 2mm. The objective is to understand the intensity of smaller hydrogen flames and verify whether the shape of the leak has a substantial influence on flame characteristics. Namely, hydrogen flame temperature, heat flux, and horizontal flame length were measured at standard flow rates between 1-5SLPM (Standard Liters Per Minute) by using five different nozzles varying in size between 0.4-1.7mm, two of which had a slot-shaped orifice representing a more crack-like leak rather than a pore-like leak. Nozzle exit-sensor spacing was also varied between 1in (25mm) up to 4in (100mm) to investigate the effects of a leaks' proximity to a surface (which is represented by the sensors) for the different leak conditions. Cases where hydrogen flames both do and do not impinge on the sensors were observed and the corresponding flame characteristics were recorded.

More importantly, this small study attempts to lay the foundation for future hydrogen flame safety experiments to come at the WJHTC FAA facility. The ultimate aim is to be more equipped and informed to tackle various challenges regarding hydrogen aircraft propulsion and be capable of regulating and creating new safety standards for this emerging technology at the FAA.

Section 2: Experimental Setup and Methods

2.1 Experimental Setup

The experimental setup consisted of three major components: a custom burner to create flames, the sensors for collecting flame data, and a rig for hoisting the sensors. A general sketch of the setup is shown in **Figure 5**. To elaborate, the main body of the burner was a 1/4in (~6.35mm) 316 stainless steel tube attached to a tank of ultra-high purity 99.99% hydrogen gas via a Tygon tube and was elevated by aluminum T-slot bars along its length to keep it horizontal and parallel with respect to the table. The tip of the pipe had a yor-lok fitting attached onto which nozzles would be inserted. A small hinge mechanism was created to hold a spark igniter and allow it to be moved or positioned as needed. The spark igniter was positioned above the nozzle exit, attached to the T-slot bars, allowing for a straightforward ignition process, as shown in **Figure 6**. The igniter was powered by a 120V ignition transformer and controlled remotely with an on/off switch.

An AX-MC-5SLPM-D Mass Flow Controller (MFC) was used for controlling hydrogen gas flow rate in the burner, **Figure 7**. Additionally, the MFC was remotely controlled via Alicat's FlowVision software. The MFC was attached downstream of the hydrogen tank and a Matheson CGA-350 Single Stage pressure regulator. The MFC allowed for direct control over the incoming flow from the regulator and by using the FlowVision software, the flow rate was easy to tune and halt when needed. The outgoing flow was delivered to the burner via a Tygon tube. A ball valve was placed as an intermediary between the Tygon tube and the burner as a redundant safety measure. A Matheson Tri-Gas Flashback Arrestor (Model 6103A-F) was placed between the

hydrogen tank regulator and the MFC as a safety measure in case of a flashback during the experiment.

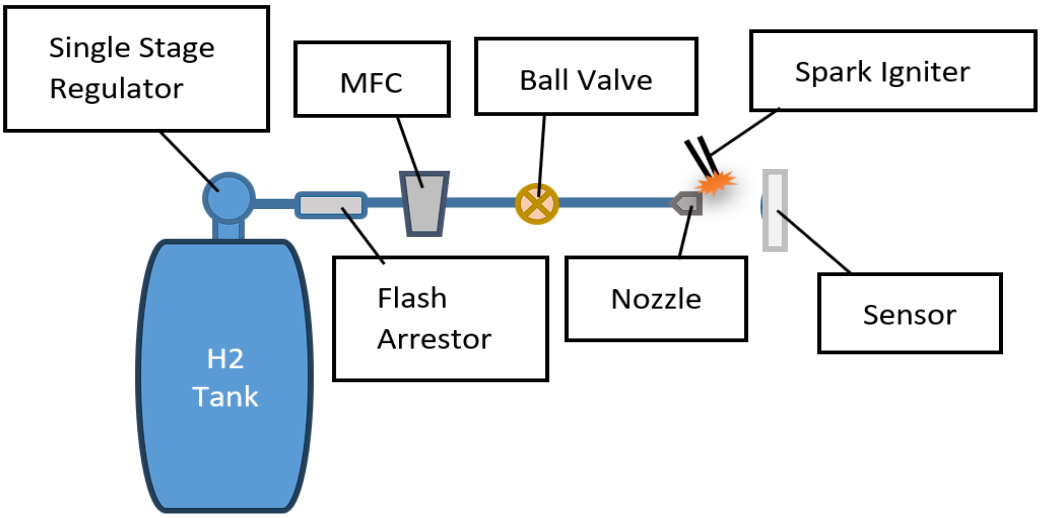

Figure 5: Sketch/Diagram of Experimental Setup

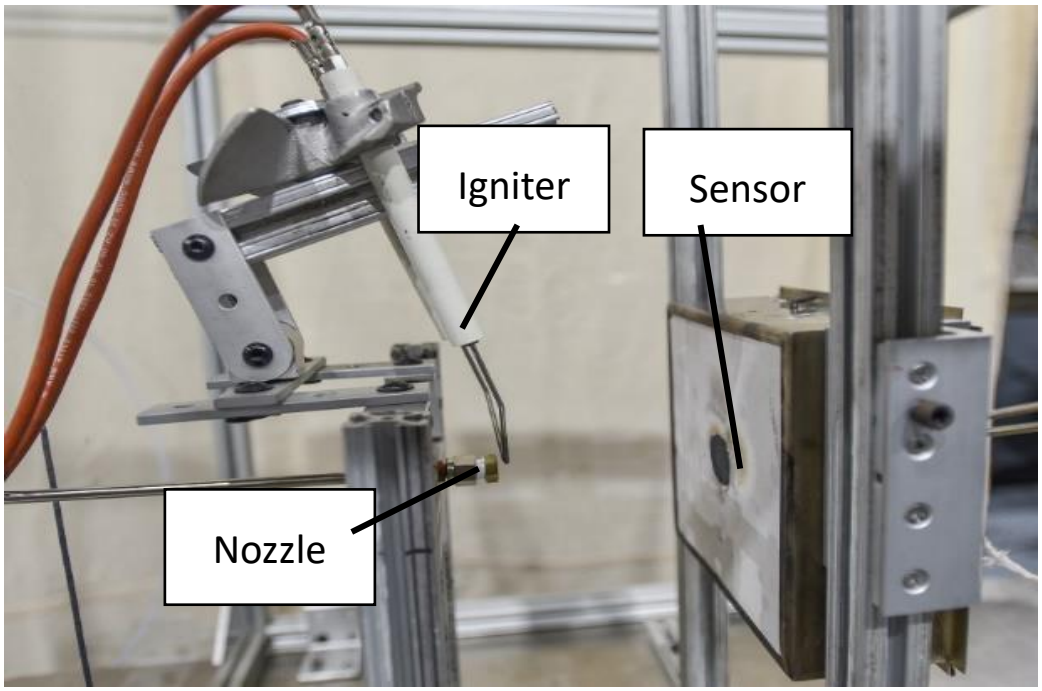

Figure 6: Close-up on Burner

Figure 7: AX-MC-5SLPM-D Mass Flow Controller

There were two sensors used for this experiment: a heat flux transducer (**Figure 8**) and a rake of seven K-type thermocouples (**Figure 9**). The heat flux transducer is also known as a water-cooled gardon gauge which was made by Vatell Corp. The surface of the gauge is covered in high temperature black paint which covers the sensor located in the center and serves as a heat sink. The gauge was attached to a water pump which circulated water through the gauge, preventing it from overheating during testing. The gauge was calibrated for roughly 9.4 W/cm^2 per mV of signal for a full-scale output of 10mV. The units could be over-drive to up to 15mV without damage or loss of calibration and results remaining valid. The K-type thermocouples (1/16in Omega KQXL) were made for use at up to roughly 2440°F. The tips of the thermocouples were bent closer to one another, spaced about 1/8in apart, to make sure to acquire good flame temperature distribution when observing the small hydrogen flames.

To keep these sensors steady, they were mounted on a movable rig to hold them upright, as illustrated in **Figure 10** and **Figure 11**. The gardon gauge was held up

horizontally by a square shaped, metal casing with white insulating material protecting the main body of the gauge, as can be seen in **Figure 6**. This gardon gauge body was mounted on a movable rig made of aluminum T-slot bars, as shown in **Figure 10**. The directions in which the rig could move are indicated by the red arrows. Similarly, the thermocouple rake was mounted on this movable rig, as shown in **Figure 11**. The mounting rigs were made this way to make sure that the sensors could be positioned in line with the hydrogen flames from the burner and make it possible to vary one of the test parameters, i.e., nozzle-sensor spacing.

Five nozzles were used in this experiment, all made of 1/4in brass plugs, all displayed in **Figure 12**. Three of the plugs were made to have circular orifices and two were made to have slot-shaped orifices and their orifice sizes are listed in **Table 1**. Each nozzle is numbered #1 through #5 and they will be referred to by their numbers in this paper.

To prevent entrainment and draft disturbances from affecting the flames, a plexiglass box was made to surround the burner and the sensors, as shown in **Figure 13**. The box allowed the burner to run with an undisturbed flame and permitted relatively smooth data acquisition.

Finally, a FLIR camera was used to detect and record the invisible hydrogen flames (such as the one shown in **Figure 2**), which helped to align the sensors properly in front of the hydrogen flames. Some flame videos captured by the FLIR camera were later used to estimate the flame length using a Flame Tracker video processing software [21].

Figure 8: Water-Cooled Heat Gauge

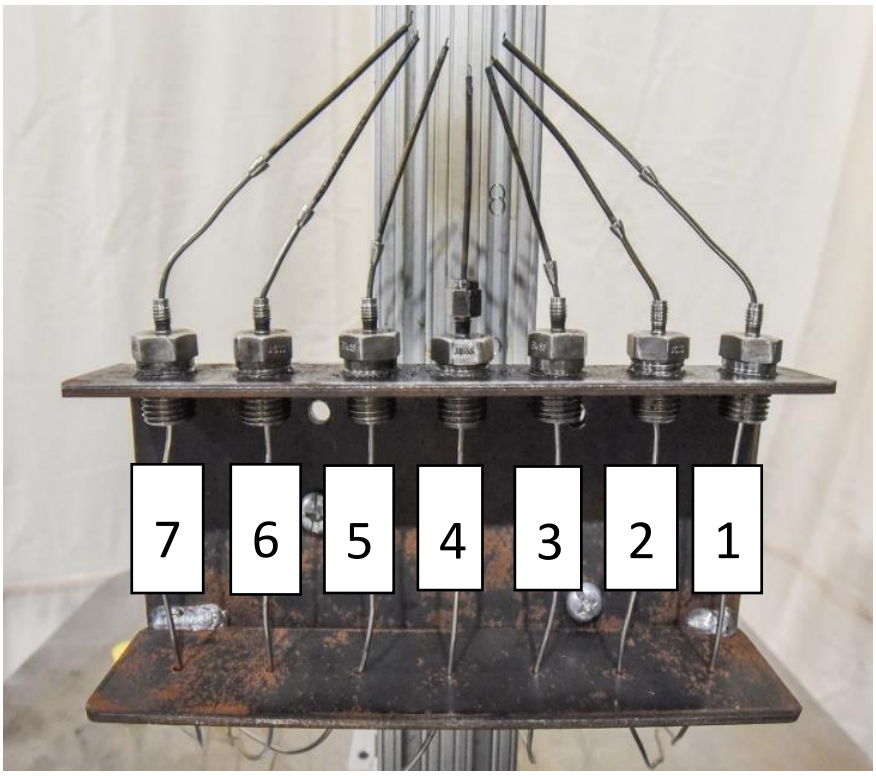

Figure 9: Thermocouple Rake

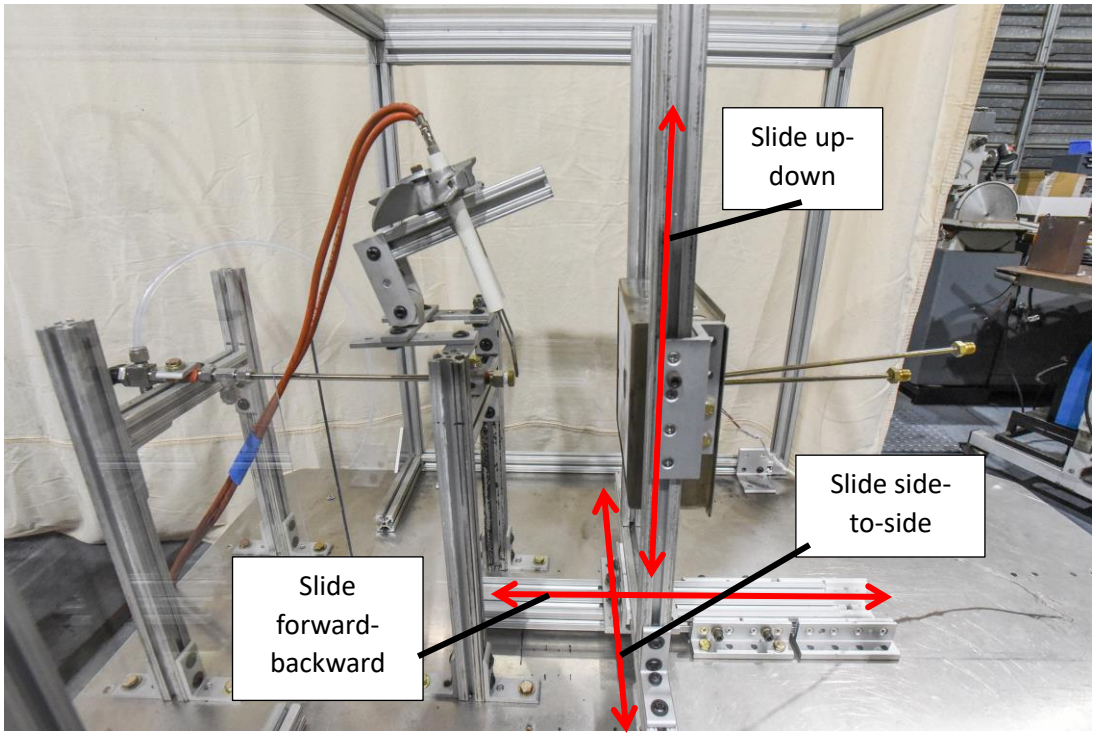

Figure 10: Movable Rig for Gardon Gauge

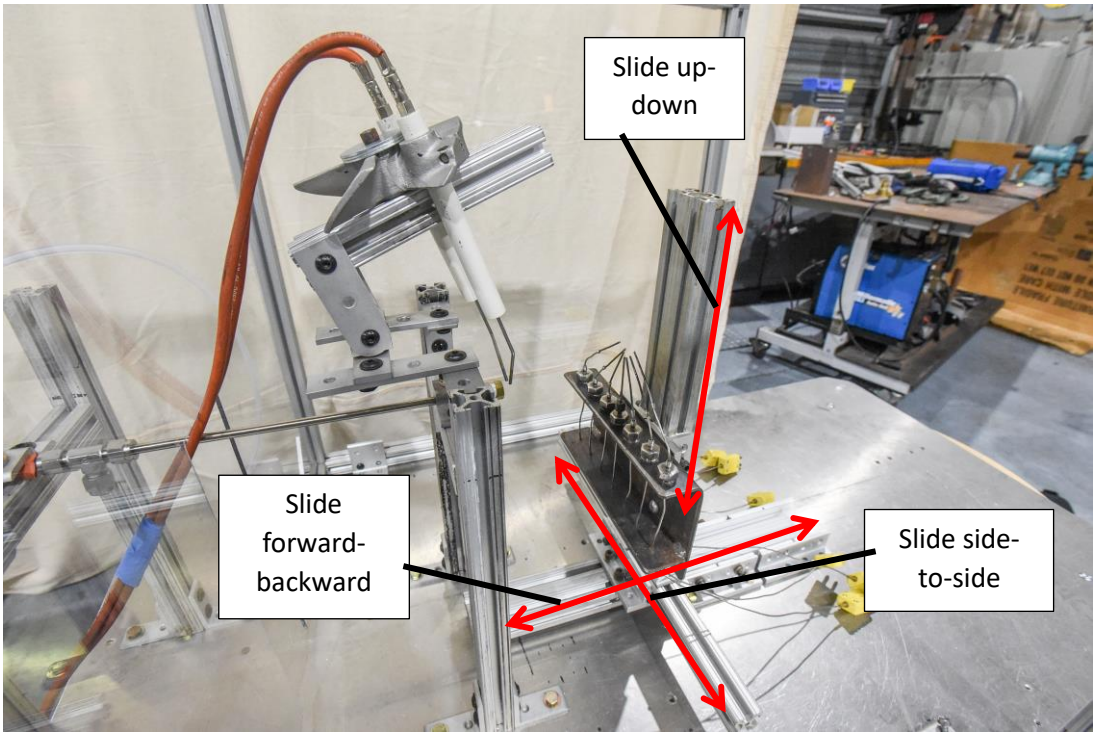

Figure 11: Movable Rig for Thermocouple Rake

Figure 12: All Nozzles Pictured and Numbered

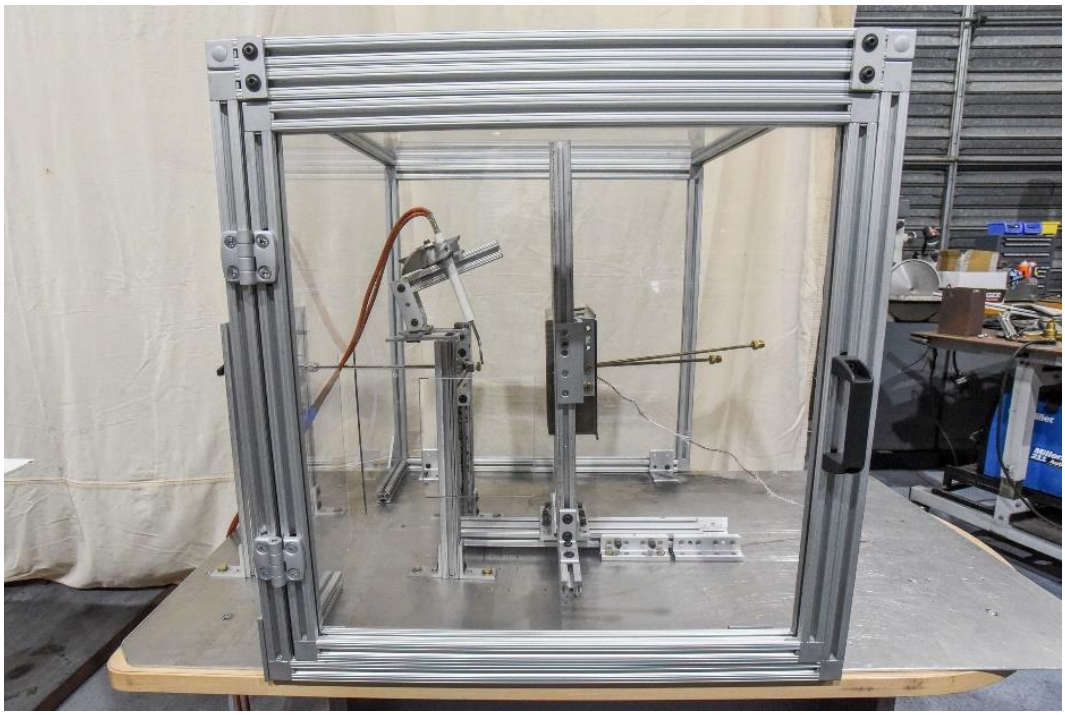

Figure 13: Burner Contained in Plexiglass Box

2.2 Test Procedure and Method of Measurement

This experiment has the following independent parameters: nozzle orifice shape, orifice size, standard flow rate (SFR), and nozzle exit-sensor spacing. For each parameter, multiple values were tested. The SFR values tried were 1SLPM, 3SLPM, and 5SLPM, the nozzle exit-sensor spacing varied were 1in (25mm), 2in (50mm), and 4in (100mm). The nozzle orifice diameters ranged from 0.4-1.7mm, (their exact sizes are listed in **Table 1**). It should be noted that nozzles #2 and #4 are nozzles of comparable orifice area, yet different orifice shapes, as well as nozzles #3 and #5. The flames produced by these two pairs of nozzles were compared and their characteristics discussed in Section 3.

Table 2 represents the test matrix that was organized and used as a guide for the test procedure. To elaborate, firstly, a nozzle was picked and the proper nozzle exit-sensor spacing established at either 4in (100mm), 2in (50mm), or 1in (25mm). Then, at that spacing, flame heat flux or flame temperature data was collected at all SFR values. Thereafter, the spacing would be adjusted and more data was collected until the test matrix was filled. Finally, the nozzle would then be interchanged and this test process repeated until all flame data was collected with all five nozzles. It is worth noting that while all tests were conducted with SFR values of 1SLPM, 3SLPM, and 5SLPM, a few additional data points were collected at 2SLPM and 4SLPM values with nozzles #2 and #3. This was done to get additional insight on an issue which was initially unclear, and this will be discussed in Section 3.2.

Before discussing the results of this experiment, it is worth noting some of the potential error factors in the data and limitations with the abovementioned sensors.

Firstly, the K-type thermocouples used in this experiment were made for use up to 2440°F, therefore it was not possible to collect hydrogen flame temperature data that may have gone beyond this limit. Similarly, because the gardon gauge has a single sensor in the center of its surface, the heat flux data collected is only representative of a single point on a given surface and not representative of what a whole impinging surface may experience. Furthermore, a few things may have affected the results. For example, during the flame tests involving the gardon gauge, some condensation formed on the surface of the gauge which could affect the sensor readings. As mentioned, the gardon gauge was perpetually cooled via a flowing water through its body, therefore the condensation formed because of a simultaneous cooling and heating of the surface of the gauge. Additionally, due to the plexiglass wall surrounding the flame and the sensors while active, the ambient temperature within the box serves as another potential error that can affect the results.

Nozzle #	Shape	Diameter		Area
-	-	[mm]	[m]	[mm^2]
1	Circular	0.4046	0.000405	0.129717
2		0.889	0.000889	0.620717
3		1.7018	0.001702	2.27461
4	Slot	0.6352	0.000635	0.596613
5		1.2704	0.00127	2.386451

Table 1: All Nozzles and Corresponding Shape, Diameter, and Area Listed

Nozzle	Spacing (in)	SFR (SLPM)	Heat Flux (W/cm^2)	Temperature (F)
#1	4	1		
		3		
		5		
	2	1		
		3		
		5		
	1	1		
		3		
		5		

Table 2: Test Matrix

Section 3: Results and Discussion

3.1 General Results and Estimation

Theoretical values of Reynolds Number and Froude Number were calculated for each nozzle and SFR (standard flow rate) combination and these values are listed in **Table 3**. These values are plotted for better illustration in **Figure 14** and **Figure 15**. The Reynolds Number ranged between *110-2400* and the Froude Number ranged between *60-10200*. As shown, nozzle #1 produced the highest Reynolds and Froude numbers, followed by nozzle #2 and #4 and #3 and #5. The flames from nozzles with the higher orifice sizes (such as, nozzles #3 and #5) yielded the smallest Reynolds and Froude numbers while the smaller orifices (such as nozzle #1) yielded the highest values. This implies that the smaller the orifice size was the more momentum dependent the hydrogen flame would be and have higher velocities, as well, while the bigger orifices produced flames with a higher degree of buoyancy effect and low velocities. The correlation between the Froude Number and the degree of buoyancy in these flames agrees with the trajectory predictions Kim [2] made. Additionally, it is deduced that while the rate of hydrogen release, i.e., the SFR, has influence on the Reynolds and Froude number values (thus, an influence on the flames' trajectories), the most influential factor was the orifice size, or the cross-sectional area of the orifice. Moreover, the shape of the orifice had little to no influence for estimating these values if the orifice size (or, area) remained unchanged.

The hydrogen flame length was also estimated, and the results are shown in **Figure 16**. The flames measured were produced from all five nozzles at SFR values of

3SLPM and 5SLPM. The flame length was regarded as the horizontal distance the flame covered from the nozzle exit up to the furthest reach of the flame. It can be observed that flame length varies widely between *79mm-162mm* depending on which nozzle and SFR was used, however, in general, it is deduced that when increasing the SFR, the flame length would also increase. Overall, the flame length greatly depended on how buoyant a flame was. Meaning, the flames with less buoyancy influence had the highest flame length while the flames with the higher buoyancy influence had the lowest flame length. And, again, the buoyancy of a flame was dependent on the orifice size and the SFR combination, which is echoed by Mogi's [8] notion that flame size depends on both nozzle size and release pressure (or, in this case, flow rate of the release). Additionally, it can be observed that the flames produced by nozzles #2 and #4 (the circular and slot nozzles of similar orifice area) were similar in length (*162mm* and *153mm*, respectively, at 5SLPM), as well as the flames produced by nozzles #3 and #5 (*142mm* and *123mm*, respectively, at 5SLPM). This implies that the orifice shape had little to no influence on the flame length.

Additionally, the nozzle exit-sensor spacing to orifice diameter ratios were calculated and these values are tabulated in **Table 4** for clarity.

Re #	Nozzle #1	Nozzle #2	Nozzle #3	Nozzle #4	Nozzle #5
1SLPM	478.4678756	217.7593954	113.754908	304.7671639	152.3835819
3SLPM	1435.403627	653.2781861	341.2647241	914.3014916	457.1507458
5SLPM	2392.339378	1088.796977	568.7745401	1523.835819	761.9179096
Fr #	Nozzle #1	Nozzle #2	Nozzle #3	Nozzle #4	Nozzle #5
1SLPM	2039.407569	287.5212594	56.70914066	353.8884761	62.5592353
3SLPM	6118.222707	862.5637783	170.127422	1061.665428	187.6777059
5SLPM	10197.03784	1437.606297	283.5457033	1769.44238	312.7961765

Table 3: Reynolds and Froude Numbers Estimations

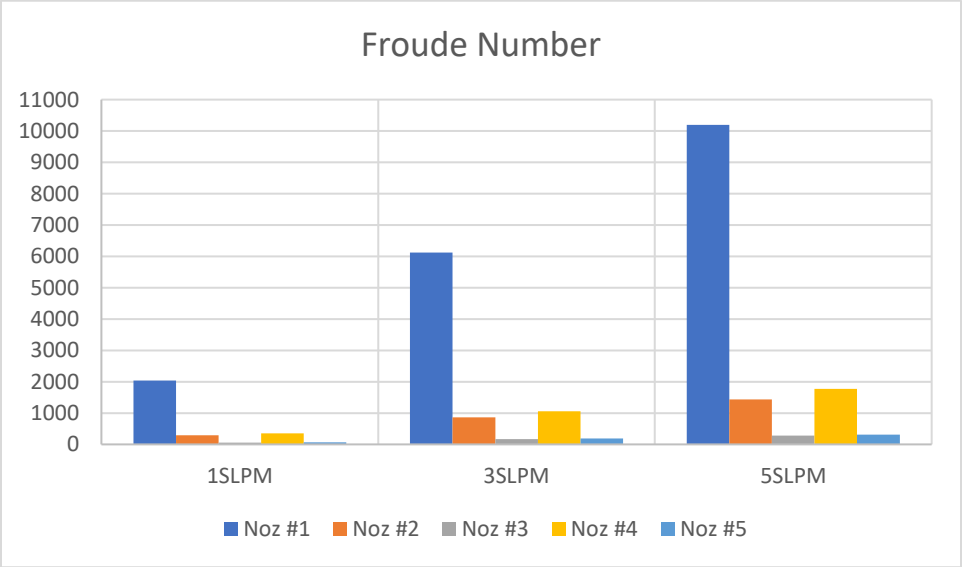

Figure 14: Estimated Froude Number for Every Nozzle/SFR Combination

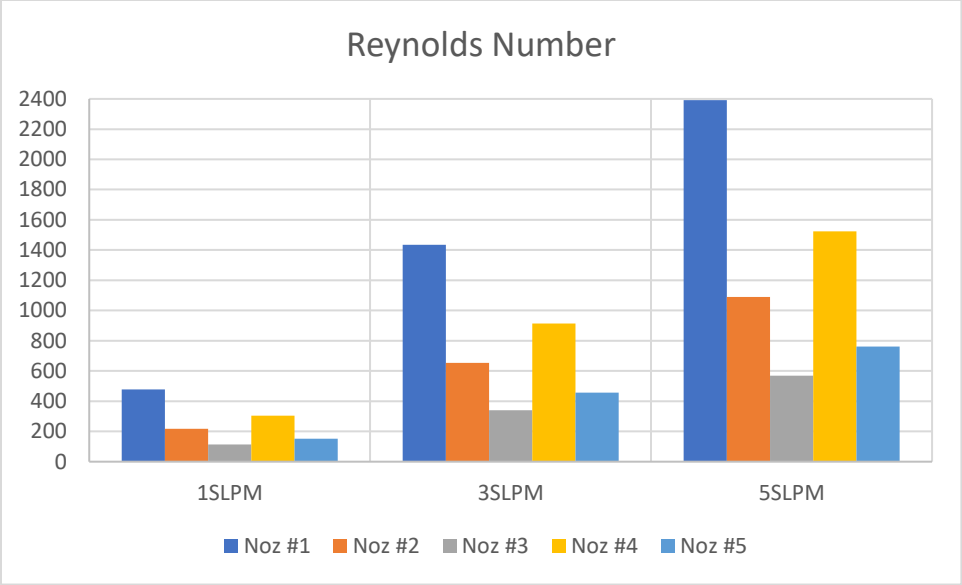

Figure 15: Estimated Reynolds Number for Every Nozzle/SFR Combination

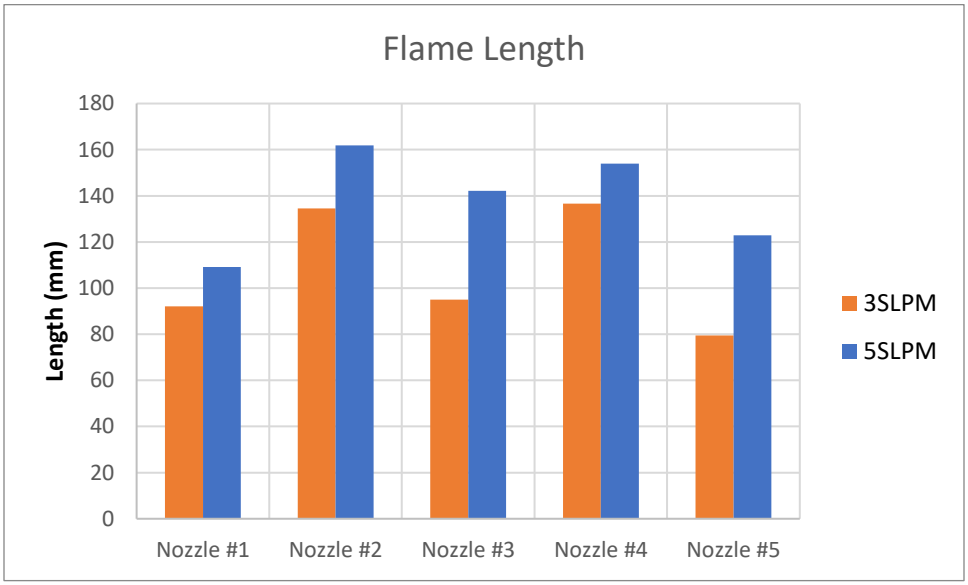

Figure 16: Hydrogen Flame Length Estimations

L/D	Spacing 1in	Spacing 2in	Spacing 4in
Nozzle #1	62.778052	125.556105	251.11221
Nozzle #2	28.571429	57.1428571	114.28571
Nozzle #3	14.925373	29.8507463	59.701493
Nozzle #4	39.987406	79.9748111	159.94962
Nozzle #5	19.993703	39.9874055	79.974811

Table 4: Ratio of Nozzle Exit-Sensor Spacing to Nozzle Diameter

3.2 Flame Heat Flux

The impinging flame heat flux tests were repeated thrice, and the results were averaged and organized into five main plots representing data collected with each of the five nozzles. **Appendix A** shows some of the raw heat flux data collected and **Figures 17(a)-(e)** show the averaged impinging heat flux data varying with respect to SFR. The three lines in each plot represent average flame heat flux at different nozzle exit-sensor spacing. In all five figures, it can be observed that, generally, increasing SFR results in an increase in average flame heat flux. Also, it can be observed that varying the spacing between the nozzle exit and the sensor also affects the flame heat flux. Namely, the shorter the spacing is, the higher the recorded heat flux becomes. For instance, in **Figure 17(a)**, the data collected with nozzle #1, it's evident that when the spacing is 4in, the heat flux recorded is around $13W/cm^2$ for all three SFR values. But when the spacing is eventually reduced to 1in, those same flames at the same SFR values produce impinging heat flux beyond $110W/cm^2$ solely due to the increase in proximity. This pattern remains consistent in the rest of the plots in **Figure 17**.

Heat flux is also affected by length, or horizontal reach, of the flames, or, in other words, the degree of buoyancy of the flames. Meaning, if a flame is highly buoyant, its reach will be shorter and, therefore, the heat transfer to the sensor (or, a surface) will be lower. In this manner, the shorter, more buoyant flames tend to make little to no contact with the sensor, especially at wider spacings, and the resulting heat flux values were very low. For instance, in **Figure 17(b)** it can be observed that for the orange line (representing the 4in nozzle exit-sensor spacing) at the 1SLPM SFR point, the resulting heat flux is $0W/cm^2$. This indicates that the flame was not long enough to reach the sensor

positioned 4in away from the nozzle for any heat transfer to occur. However, if the SFR is increased to, say 3SLPM, the heat flux reaches about $33W/cm^2$, or if the spacing is reduced, for example, to 1in, then the heat flux reaches about $30W/cm^2$, as well. Similar observations can be made in the rest of **Figure 17**. Changing these parameters further results in further increase in flame heat flux, in general. Meaning, theoretically, continuing to increase SFR and reducing spacing will result in higher and higher heat flux, however, **Figures 17(b)-(e)** indicate otherwise.

As explained in Section 1.3, there are a few main regions along the full length of a flame. Namely, the potential core zone and the free jet zone, in addition to the impingement zone in case an impinging wall is present. As aforementioned, the potential core zone is a region of incomplete combustion containing a lot of unburned hydrogen gas while the free jet zone and beyond is a region with complete hydrogen combustion. Varying the parameters such as orifice size and SFR will effectively vary the size of each of these flame zones. The greater the size of an orifice and the higher the flow rate of hydrogen becomes, the bigger the unburned and burned gas zones become, correspondingly. Leading back to **Figures 17(b)-(e)**, it can be observed that the blue line (representing the 1in nozzle exit-sensor spacing) in each figure begins to dip after the 3SLPM SFR point. For instance, observing **Figure 17(b)**, the blue line at the 3SLPM point shows a corresponding average heat flux value of about $95W/cm^2$ and as the SFR is eventually increased to 5SLPM, the heat flux value at that point is about $64W/cm^2$, which is roughly a *30% decrease* in heat flux at the spacing of 1in (25mm). This data represents the flame produced by nozzle #2 and the data for all other nozzles (except for nozzle #1) show a similar decrease in heat flux going from 3SLPM to 5SLPM at the 1in nozzle exit-

sensor spacing. The reason being that increasing the SFR from 3SLPM to 5SLPM results in an increase in the size of the potential core zone and, therefore, this zone containing a lot of cold, unburned hydrogen gas makes more of a contact with the sensor which results in the impinging heat flux to be lower than initially expected. Of course, when the spacing is increased from that point, the heat flux increases. For instance, in **Figure 17(b)**, moving vertically from the blue point at 5SLPM up to the grey and orange points (each representing the 2in (50mm) and 4in (100mm) spacings, respectively, at 5SLPM), an increase in impinging heat flux up to 129W/cm^2 can be observed, up from *64W/cm^2*. This implies that the sensor was moved outside of the potential core zone into the free jet zone going beyond 1in spacing. This shift in heat flux going from the potential core zone to the free jet zone is consistent with Panda's [14] finding wherein the region which emits the highest heat flux is 70-80% up along the full length of the flame, which here is regarded as the free jet zone.

It is worth noting that a few additional test runs were conducted with nozzle #2 and #3 at SFR values of 2SLPM and 4SLPM at 1in spacing configuration to help validate the reasoning explained above. Hence why **Figure 17(b)** and **Figure 17(c)** contain blue lines with a five-point distribution instead of the common three-point distribution.

As mentioned above, the flame produced by nozzle #1 was an exception to this "phenomenon" as no stark decrease in heat flux can be observed in **Figure 17(a)**. The reasoning here being that due to the tiny orifice size of nozzle #1, there was much less hydrogen gas being released compared to what the other nozzles released at any SFR. Because of this, what little gas released from nozzle #1 would be more readily and completely burned, making the effective potential core zone much smaller and resulting

in no recording of a “colder” flame at the 1in spacing. However, in theory, if the spacing was further reduced below 1in, a contact between the potential core zone and the sensor could be established, therefore resulting in a lowered heat flux for the nozzle #1 flames, as well, in the same manner as discussed above.

Finally, it is worth noting the effects (or lack thereof) of orifice size and shape on the resulting impinging flame heat flux. Namely, looking at **Figure 17**, it can be observed that nozzle #1 (the nozzle with the smallest orifice) produces flames which potentially reach up to about $142W/cm^2$ in heat flux while the subsequent nozzles produce flames with half or third as much of a heat flux. This implies that increasing the orifice size while keeping the SFR constant produces a reduction in heat flux. The reasoning here being that an increase in cross-sectional area of a nozzle leads to a reduction in flow velocity through that orifice, therefore effectively reducing the heat transfer to the sensor from the flame. For more clarity, **Figure 18(a)-(c)** directly compares all the nozzles in terms of the flame heat flux produced, each plot representing a different spacing position. Each of the colored lines represents the different nozzles.

As an added note for clarity, the flames produced by nozzle #1 can be compared to the flames blow torches can produce, for example, wherein the flame is small, intense, and concentrated at a single point, thus producing high heat transfer qualities for cutting metals or other materials. By increasing the size of the nozzle, a blow torch will therefore become less capable for cutting due to the reduced flame concentration and intensity.

Figure 17: Average Heat Flux Data

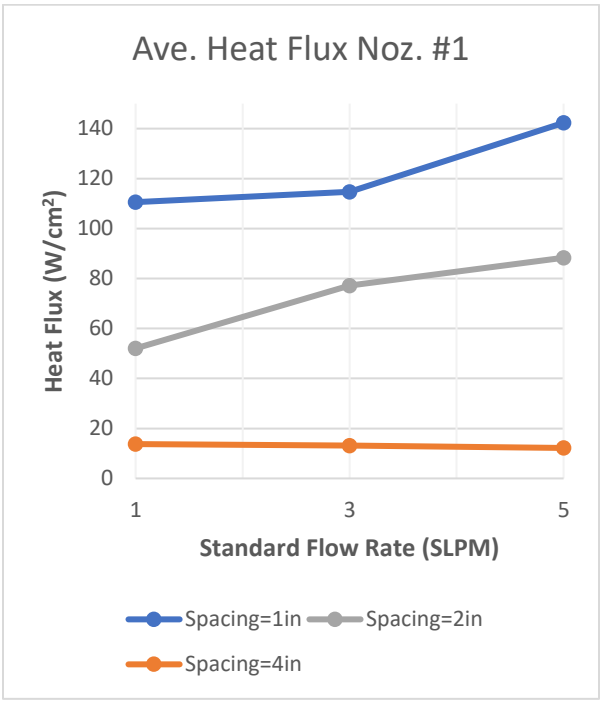

(a)

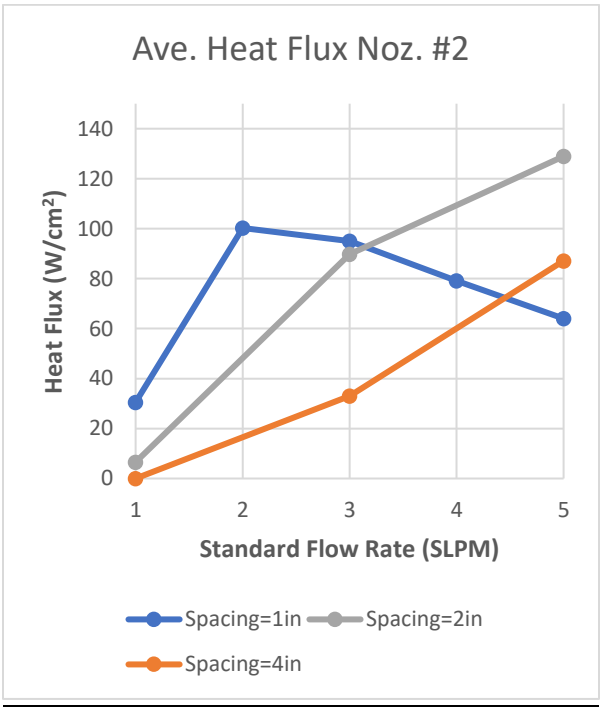

(b)

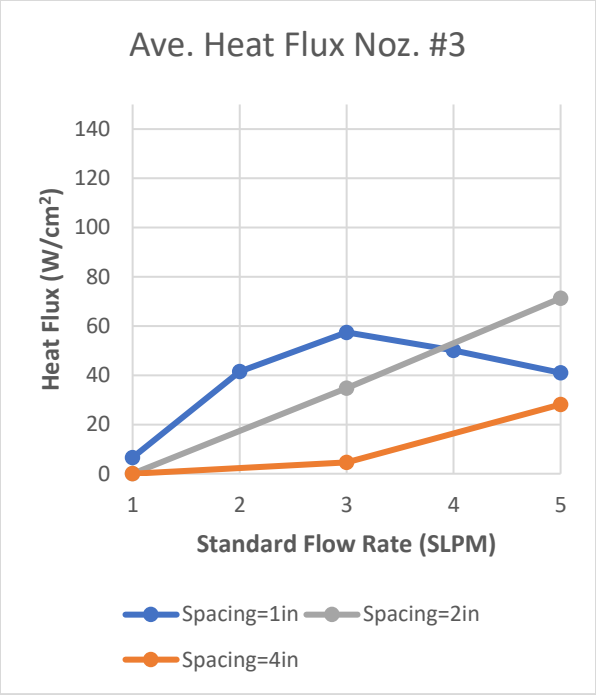
Ave. Heat Flux Noz. #3
Heat Flux (W/cm²)
140
120
100
80
60
40
20
0
1
2
3
4
5
Standard Flow Rate (SLPM)
Spacing=1in
Spacing=2in
Spacing=4in

(c)

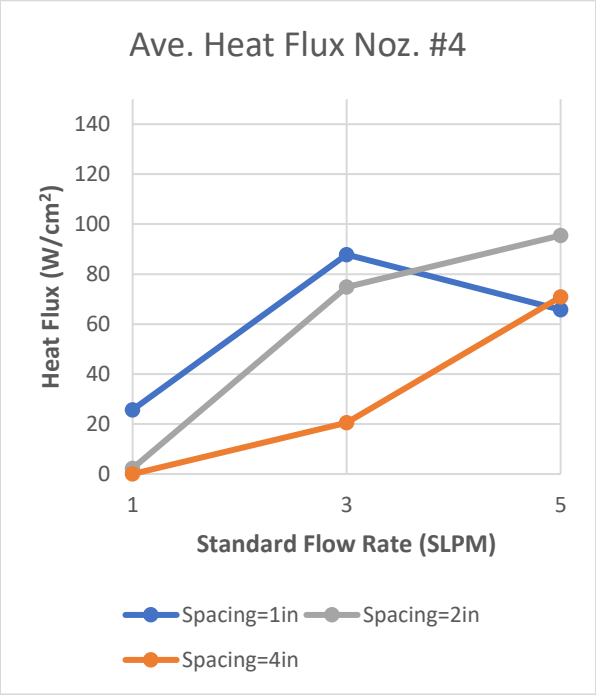
Ave. Heat Flux Noz. #4
Heat Flux (W/cm²)
140
120
100
80
60
40
20
0
1
3
5
Standard Flow Rate (SLPM)
Spacing=1in
Spacing=2in
Spacing=4in

(d)

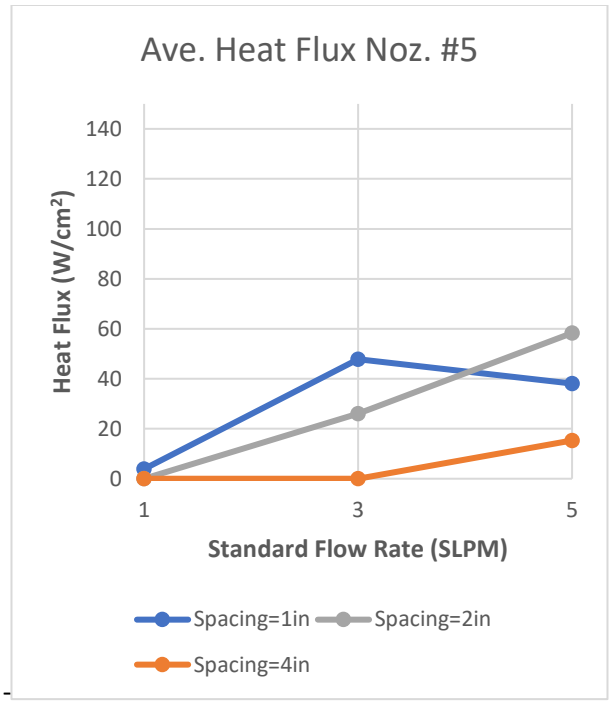

(e)

Figure 18: Nozzle Comparison for Flame Heat Flux

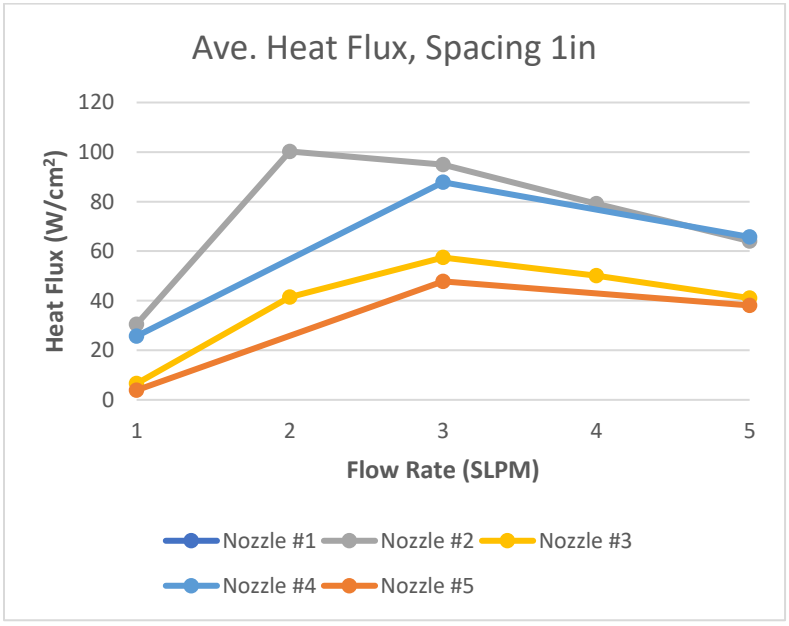

(a)

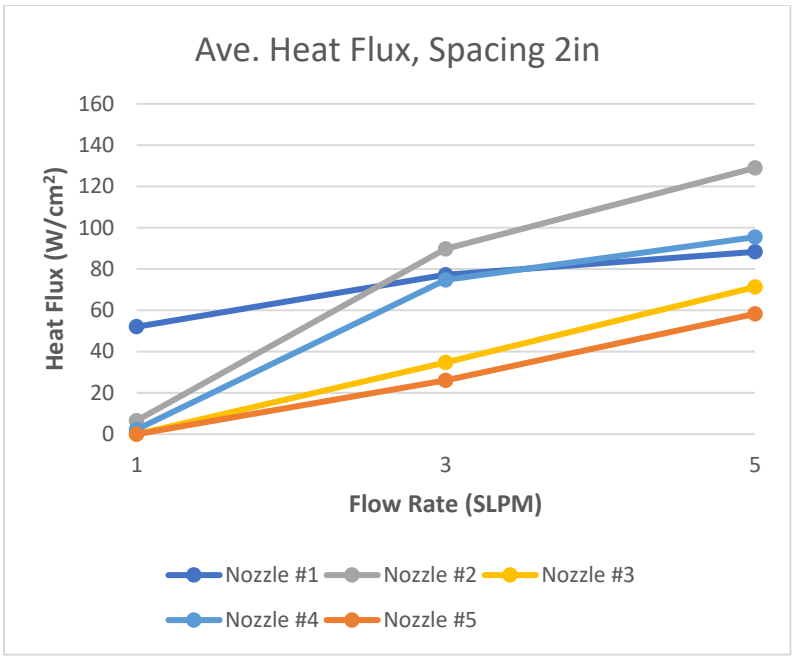
Ave. Heat Flux, Spacing 2in
Heat Flux (W/cm²)
160
140
120
100
80
60
40
20
0
1
3
5
Flow Rate (SLPM)
Nozzle #1
Nozzle #2
Nozzle #3
Nozzle #4
Nozzle #5

(b)

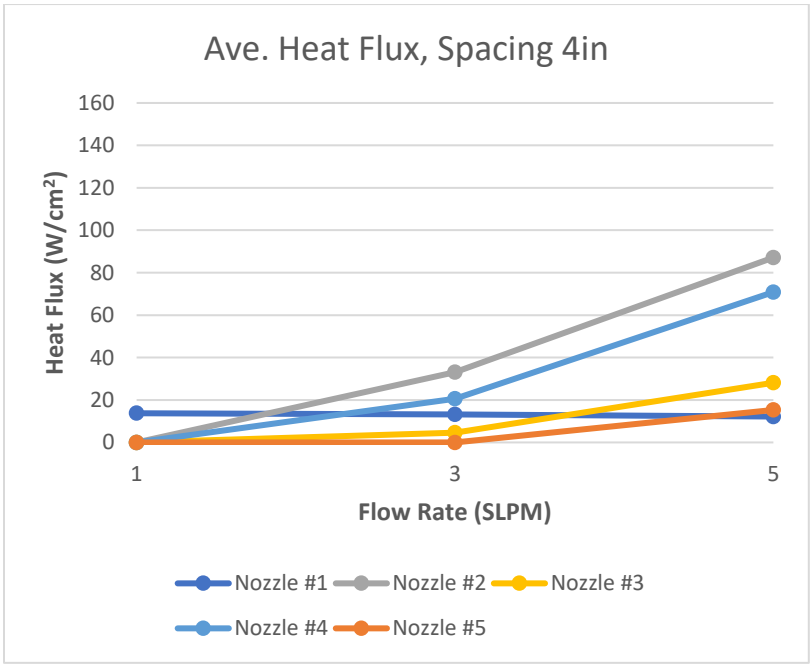
Ave. Heat Flux, Spacing 4in
Heat Flux (W/cm²)
160
140
120
100
80
60
40
20
0
1
3
5
Flow Rate (SLPM)
Nozzle #1
Nozzle #2
Nozzle #3
Nozzle #4
Nozzle #5

(c)

3.3 Flame Temperature

The temperature tests were conducted with a thermocouple rake to acquire cross-sectional flame temperature data at different nozzle exit-sensor spacings and the results were averaged and organized into several plots. **Appendix B** shows some of the raw temperature data collected and **Figure 19** through **Figure 23** represent the averaged flame temperature data calculated, each figure corresponding with data collected with each of the different nozzles. In each histogram, the colored bars represent the seven different thermocouples, and they are numbered in correspondence with the thermocouples shown in **Figure 9**. In addition, each mini-histogram in every plot represents hydrogen flames at different SFR values, while each plot represents data collected at different nozzle exit-sensor spacing.

First thing that can be observed in these figures is that each histogram has a good normal distribution where typically the central thermocouples (TC3, TC4, and TC5) picked up the highest flame temperatures while the outside thermocouples picked up lower temperatures. This, of course, implies that, generally, the hydrogen flame tends to be the hottest in the center and colder at the outer regions of the flame. Additionally, it can be observed that increasing SFR results in an increase in temperature, in general. For instance, in **Figure 20(a)-(c)** (representing flames produced with nozzle #2), increasing SFR from 1SLPM up to 5SLPM, there is a rise in the recorded flame temperature. For example, in **Figure 20(b)**, the temperature range at 1SLPM SFR is about *187-1450°F* while at 5SLPM SFR, the temperature range increases to *294-2065°F* based on the thermocouples' positions. Additionally, a general rise in temperature can be observed when the nozzle exit-sensor spacing is increased from 1in (25mm) up to 4in (100mm)

(**Figures 20(a)-(c)**). At spacing of 1in (25mm) (**Figure 20(c)**), the maximum flame temperature recorded was up to *1979°F*. When widening the spacing up to 4in (100mm), the maximum flame temperature recorded at this point goes over *2405°F*, which is over a *20% increase* in temperature while the SFR values are kept the same. These general variations in flame temperature can be observed in the other figures, as well. This temperature variation with spacing implies that along the full length of a hydrogen flame, the hottest regions are near the tip of the flame. In other words, the free jet zone of a flame is the higher temperature region while the potential core zone of a flame is the lower temperature region, which is what was already explained in the previous sections and is supported by Panda's [14] finding and discussed by Chander [10] and Dong [11] in their flame analysis.

In terms of orifice size, it's observed that nozzles with the smaller orifices produce flames with higher temperatures. Namely, nozzle #1 (**Figure 19**), produces flames that can well-surpass 2400°F in temperature while bigger nozzles such as #3, #4, and #5 (**Figures 21-23**) produce flames that reach up to *1800°F-2200°F*, depending on the nozzle. These temperature results tend to correspond with the heat flux results, wherein both the temperature and heat flux values tend to be lower for the hydrogen flames produced by nozzles of larger size. Again, for clarity, the example of the blow torch can be invoked here to comprehend the more robust flame characteristics of flames produced by smaller nozzles.

It is worth noting that in some of the figures there are missing histograms, such as in **Figure 20(c)**, the histogram for the SFR of 1SLPM is missing. The reasoning for this is that, again, some of the hydrogen flames produced were more buoyant than others,

therefore shorter, and thus little to no contact was established between these buoyant flames and the sensors. Or, for **Figure 19(a)** where data is missing for several of the thermocouples for the 3SLPM and 5SLPM mini-histograms. In these instances, the flame temperatures were beyond the limits of the K-type thermocouples (2440°F), thus the result was an error prompt. Therefore, for future tests, higher temperature range thermocouples should be utilized to better assess more intense hydrogen flame characteristics.

Figure 19: Ave. Flame Temperature w/ Nozzle #1

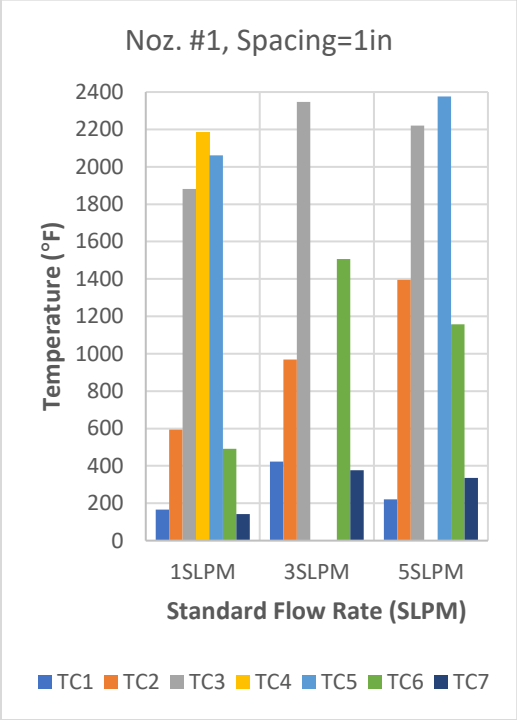

(a)

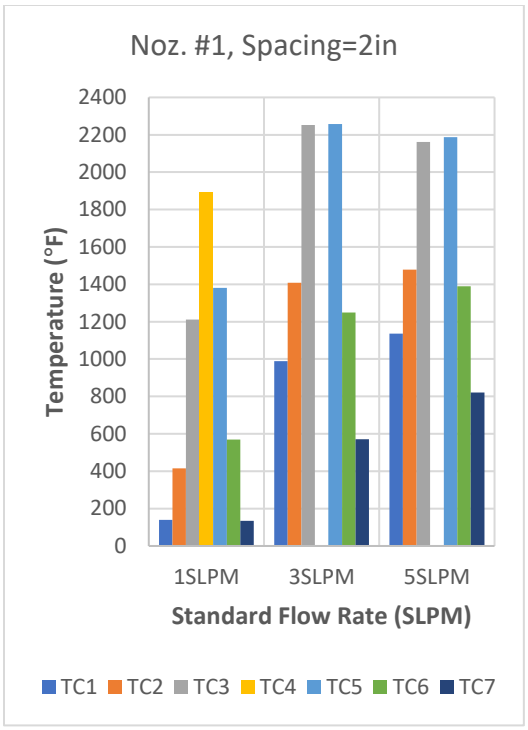
Noz. #1, Spacing=2in
Temperature (°F)
2400
2200
2000
1800
1600
1400
1200
1000
800
600
400
200
0
1SLPM
3SLPM
5SLPM
Standard Flow Rate (SLPM)
TC1 TC2 TC3 TC4 TC5 TC6 TC7

(b)

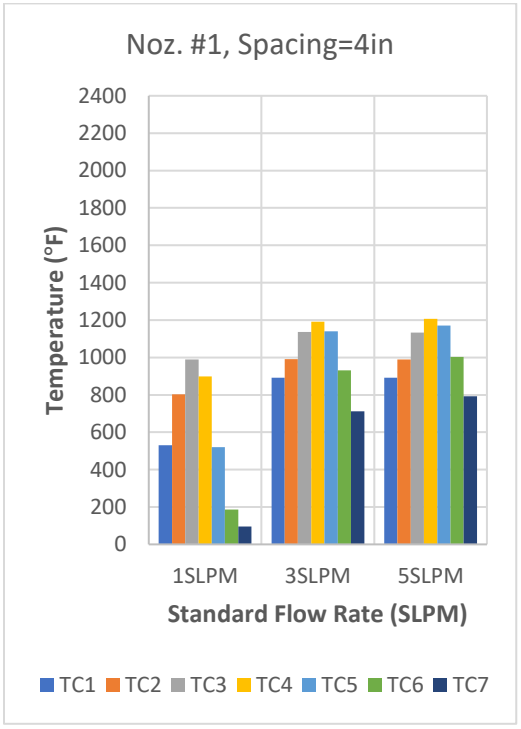
Noz. #1, Spacing=4in
Temperature (°F)
2400
2200
2000
1800
1600
1400
1200
1000
800
600
400
200
0
1SLPM
3SLPM
5SLPM
Standard Flow Rate (SLPM)
TC1 TC2 TC3 TC4 TC5 TC6 TC7

(c)

Figure 20: Ave. Flame Temperature w/ Nozzle #2

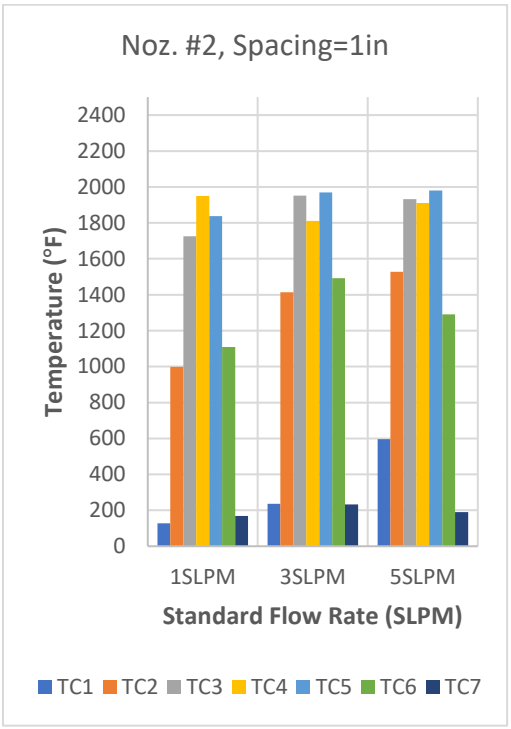

(a)

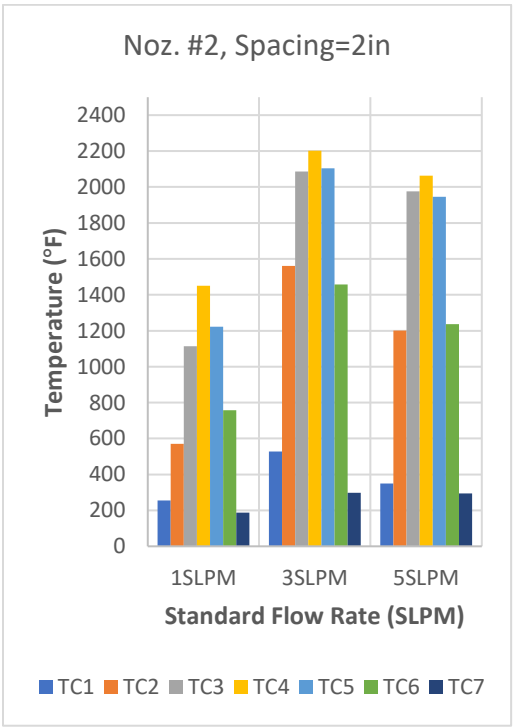

(b)

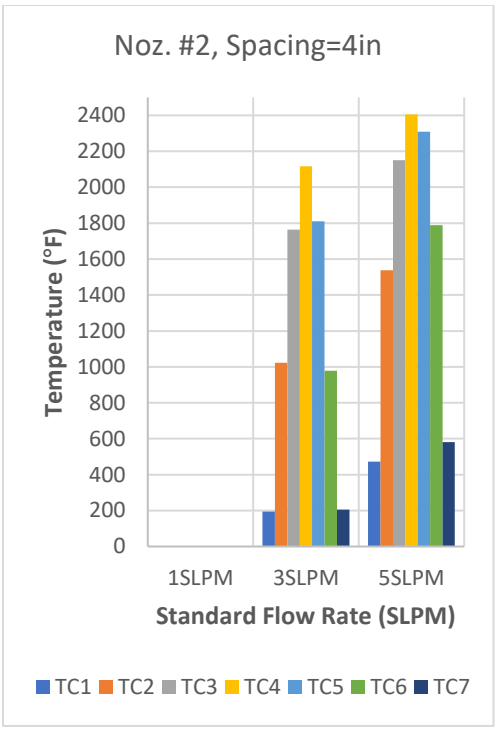

(c)

Figure 21: Ave. Flame Temperature w/ Nozzle #3

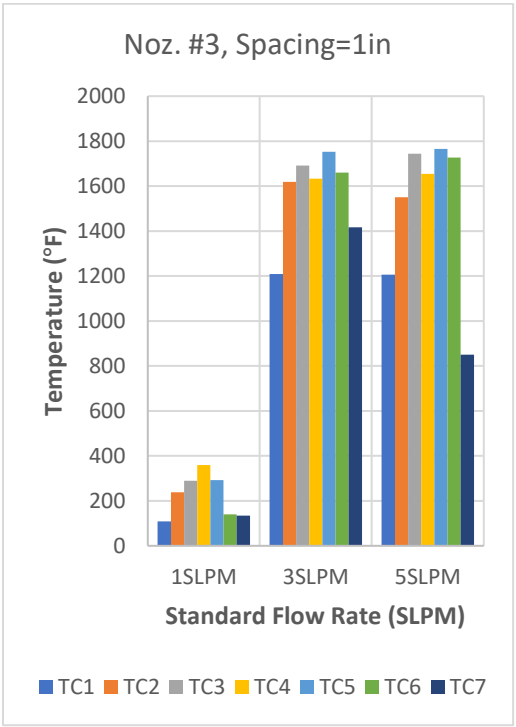

(a)

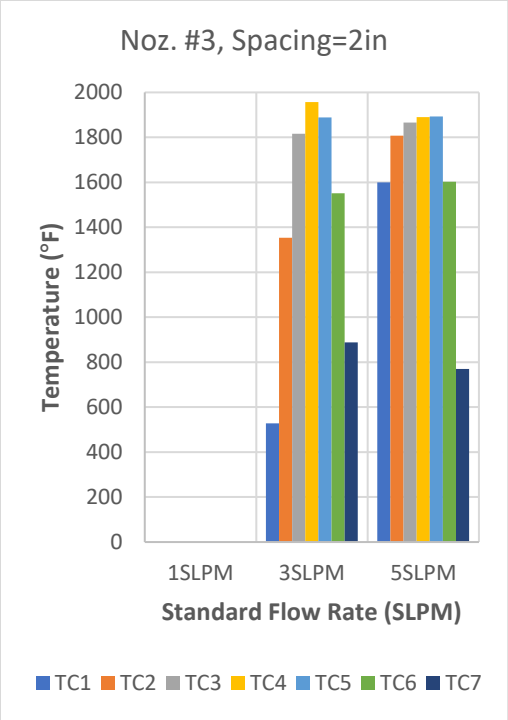
Noz. #3, Spacing=2in
Temperature (°F)
2000
1800
1600
1400
1200
1000
800
600
400
200
0
1SLPM
3SLPM
5SLPM
Standard Flow Rate (SLPM)
TC1 TC2 TC3 TC4 TC5 TC6 TC7

(b)

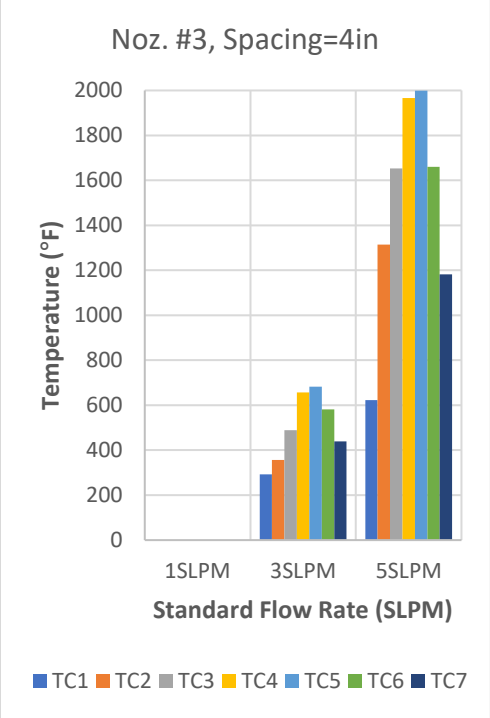
Noz. #3, Spacing=4in
Temperature (°F)
2000
1800
1600
1400
1200
1000
800
600
400
200
0
1SLPM
3SLPM
5SLPM
Standard Flow Rate (SLPM)
TC1 TC2 TC3 TC4 TC5 TC6 TC7

(c)

Figure 22: Ave. Flame Temperature w/ Nozzle #4

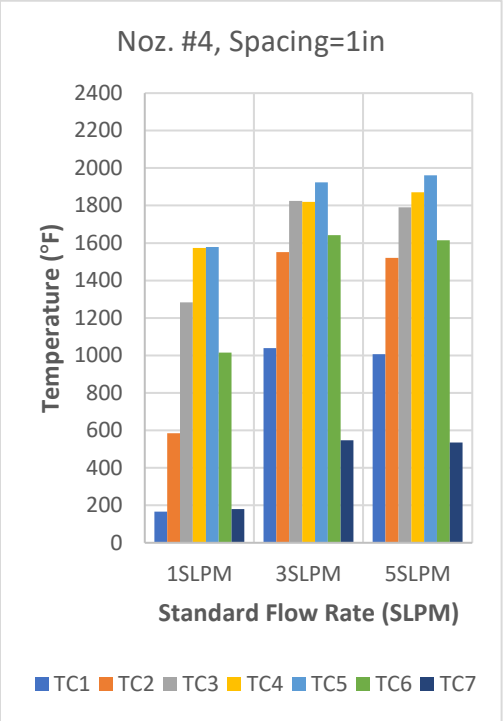

(a)

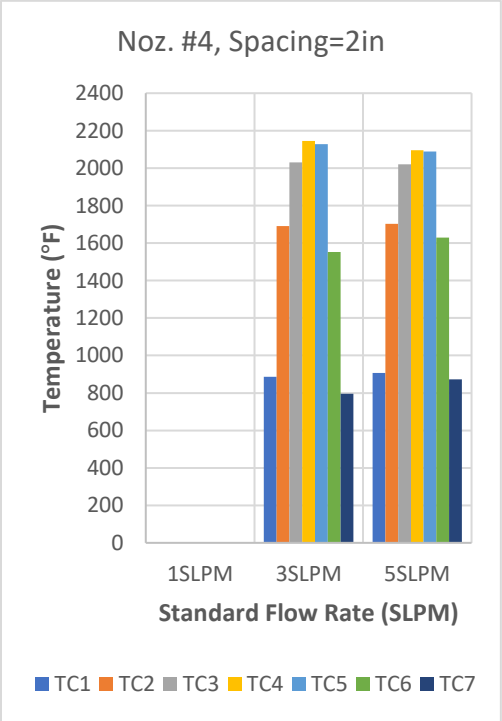

(b)

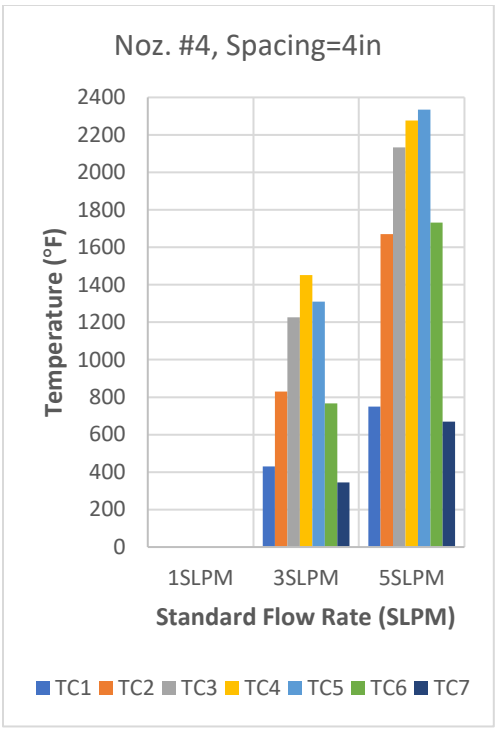

(c)

Figure 23: Ave. Flame Temperature w/ Nozzle #5

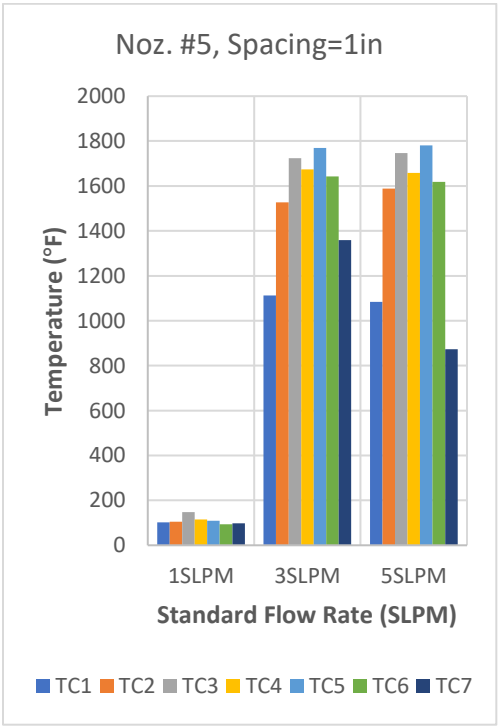

(a)

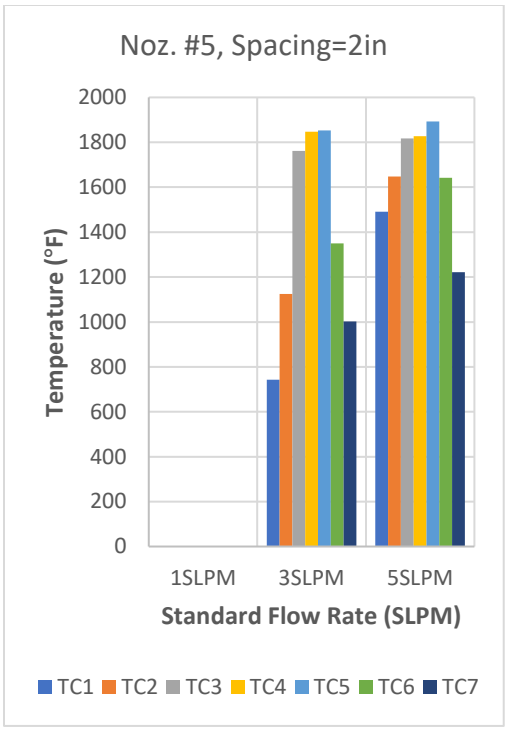
Noz. #5, Spacing=2in
2000
1800
1600
1400
1200
1000
800
600
400
200
0
Temperature (°F)
1SLPM
3SLPM
5SLPM
Standard Flow Rate (SLPM)
TC1 TC2 TC3 TC4 TC5 TC6 TC7

(b)

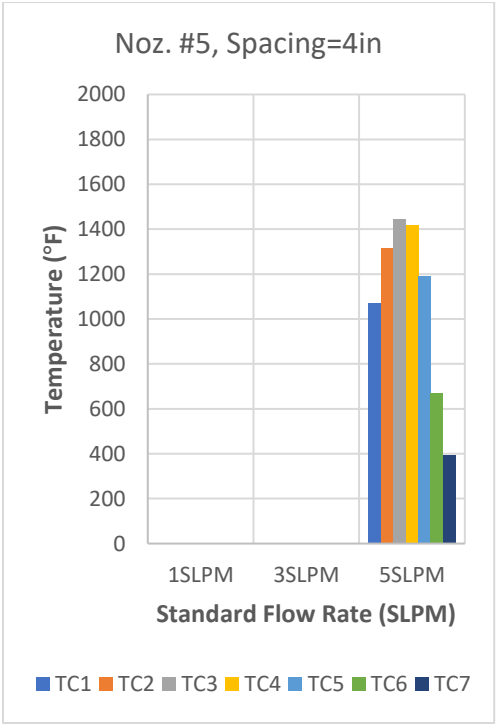
Noz. #5, Spacing=4in
2000
1800
1600
1400
1200
1000
800
600
400
200
0
Temperature (°F)
1SLPM
3SLPM
5SLPM
Standard Flow Rate (SLPM)
TC1 TC2 TC3 TC4 TC5 TC6 TC7

(c)

3.4 Circular vs. Slot Orifice Shape

As mentioned in Section 3.1, the shape of the orifice (or, the leak) had little influence on the flame length. Below in **Figure 24** and **Figure 25** a direct comparison is made between the flames produced by the circular nozzles versus the flames produced by slot nozzles and the average impinging heat flux they produced. **Figure 24** compares nozzles #2 and #4 both of which had orifice areas of around ~0.6mm^2, while **Figure 25** compares nozzles #3 and #5, both having orifice areas of around ~2.3mm^2. As can be observed in these figures, in most cases, the orange bars (representing the circular nozzles) produced flames with the higher heat flux at all SFR values. However, ultimately the difference between the two different orifice shapes is relatively marginal. The largest difference is observed to be in **Figure 24(b)** at the 5SLPM SFR value where the orange bar (circular nozzle) reaches about *129W/cm^2* while the counterpart blue bar (slot nozzle) reaches *95W/cm^2*. Otherwise, the differences between the blue and orange bars vary between *3W/cm^2* up to about *20W/cm^2* (most of them having a difference of less than *15W/cm^2*). This again infers that generally the shape of the orifice (or the leak) has little influence on hydrogen flame characteristics, which agrees with what Hecht [3] deduced. Instead, the more influential parameters are the orifice size and SFR. Ultimately, what matters is how much volume of gas is being released and how fast, not in what "shape" or "form" the gas is being released.

Figure 24: Circular vs. Slot Shaped Orifice Comparison – Nozzles #2 vs. #4

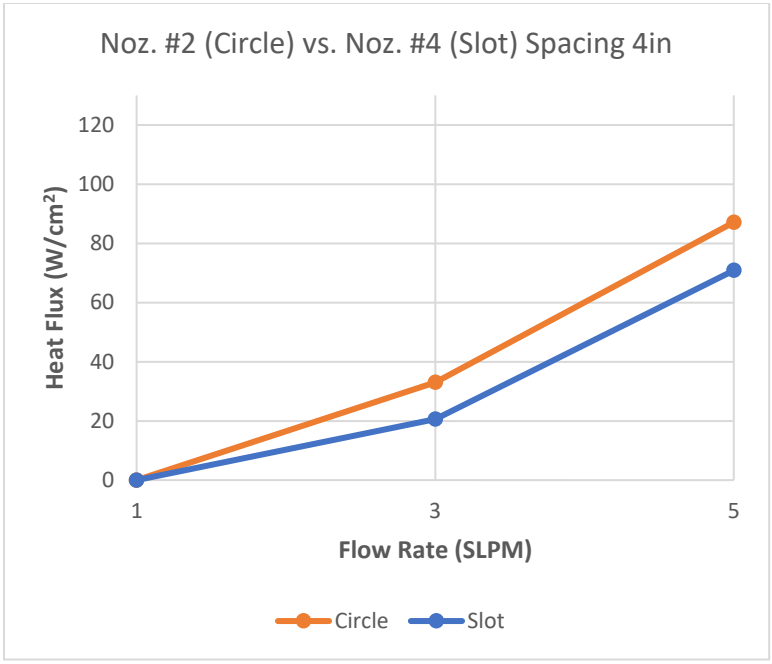

(a)

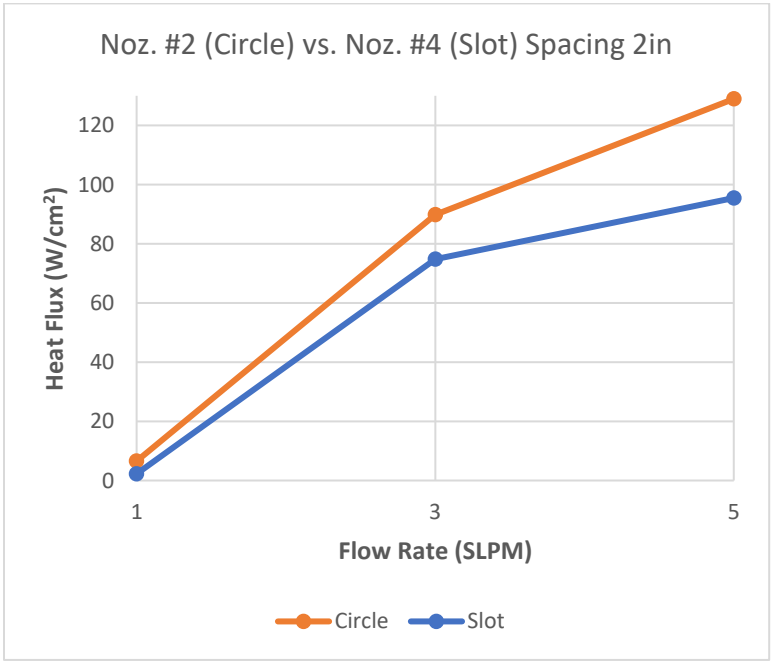

(b)

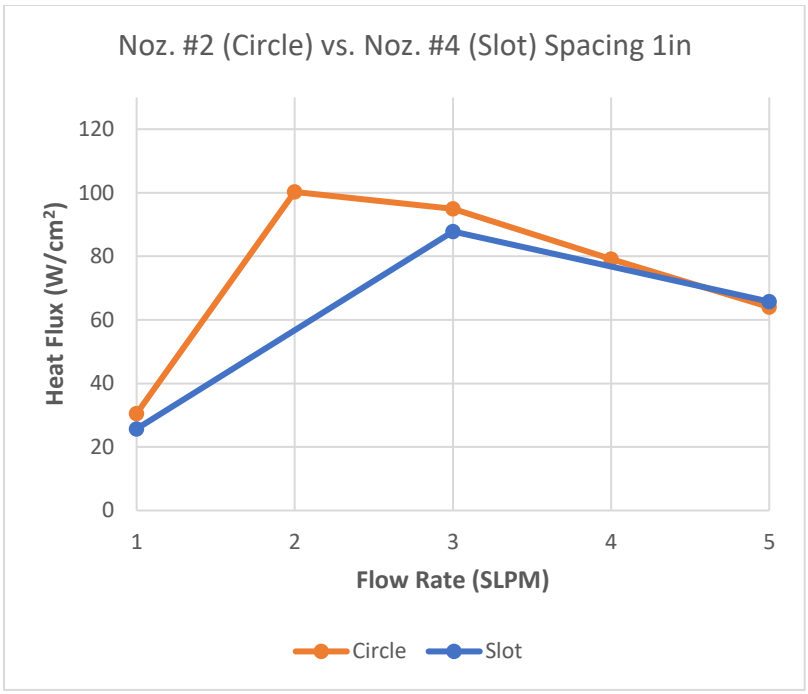

(c)

Figure 25: Circular vs. Slot Shaped Orifice Comparison – Nozzles #3 vs. #5

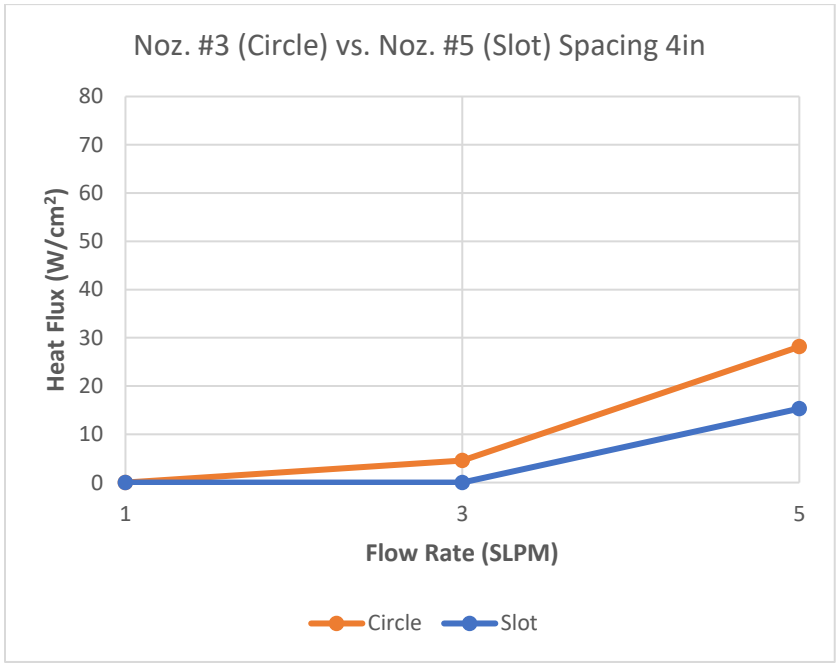

(a)

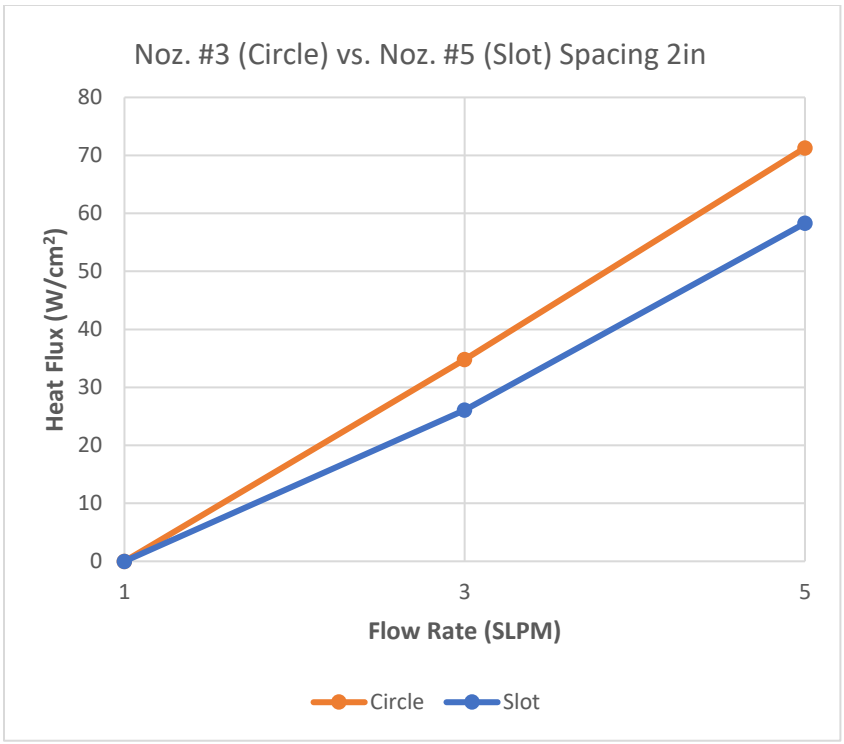
Noz. #3 (Circle) vs. Noz. #5 (Slot) Spacing 2in
Heat Flux (W/cm²)
80
70
60
50
40
30
20
10
0
1
3
5
Flow Rate (SLPM)
Circle
Slot

(b)

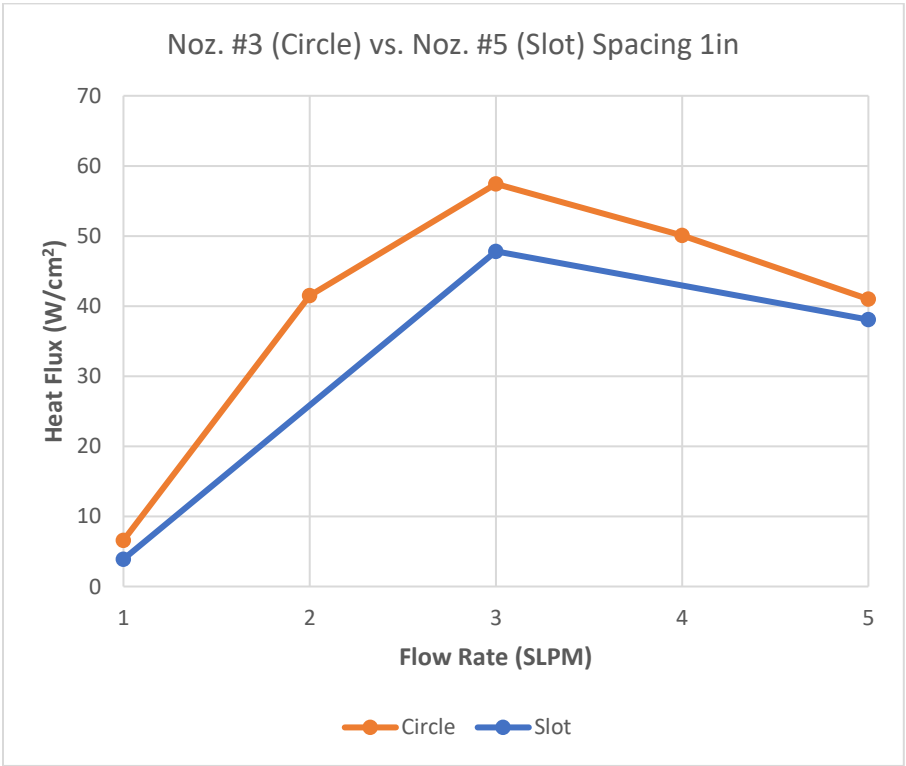
Noz. #3 (Circle) vs. Noz. #5 (Slot) Spacing 1in
Heat Flux (W/cm²)
70
60
50
40
30
20
10
0
1
2
3
4
5
Flow Rate (SLPM)
Circle
Slot

(c)

Section 4: Conclusion

The objective of this project was to study the basic flame characteristics of small leak hydrogen flames. Using a custom hydrogen burner, various leak conditions were simulated, varying the leak size and shape, leak flow rate, and leak-to-surface proximity. Impinging flame heat flux and cross-sectional flame temperature were recorded at three different nozzle exit-sensor spacings (1in, 2in, and 4in spacings) at standard flow rates of 1SLPM, 3SLPM, and 5SLPM for leak sizes between 0.4-1.7mm. Additionally, the flame length was also estimated. Results show that the shape of a leak has little to no influence on the flame characteristics, whereas the leak size and leak flow rate have the greatest effect on how a hydrogen flame behaves and the flame characteristics it induces.

The estimated flame jet Reynolds number varied between *110-2400* and Froude number varied between *60-10200*. The upper limits of the Reynolds and Froude numbers represent the smaller leaks with higher flow rates which exhibited the least buoyancy dependence. Consequently, the flames with the least buoyancy dependence tended to be the longest in horizontal reach as well as highest in flame heat flux and flame temperature, which agrees with previous studies in literature. The highest impinging heat flux recorded was $142 W/cm^2$ with the smallest nozzle #1 (diameter of 0.4046mm) at SFR of 5SLPM while some of the lowest heat flux recorded ranged between $0\text{-}13 W/cm^2$, which was also reliant on the nozzle exit-sensor spacing. The spacing was crucial for whether heat transfer to the sensors could be established, thus if the sensors were out of reach of the flames, the recorded heat flux and temperature would be low. Highest cross-sectional flame temperature recorded was up to *2376°F*, which was with nozzle #2 (diameter 0.889mm) at 5SLPM. The cross-sectional temperature also varied within a

given flame, where the highest temperatures were exhibited in the center while the lowest temperatures recorded were near the outward edges of the flame. It was also noted that the flame heat flux and flame temperature are lower in the flames' potential core zone. The transition between the free jet to the potential core zone can result in roughly a *30% decrease* in flame heat flux.

Some potential sources of error for the data may include the condensation buildup on the surface of the gardon gauge and an increased ambient temperature inside the plexiglass box during the tests. Additionally, the sensors used were limited in range, however the data collected was still valuable and good qualitative deductions were established which were consistent with other results in the literature.

For future work, more robust sensors will be utilized which are better suited for assessing hydrogen flames, while minimizing the sources of error from affecting the data, in addition to expanding the general scope of the tests. Potential future test considerations for the FAA Fire Safety Branch at the WJHTC center include hydrogen flame detectability, hydrogen flame material testing, post-crash hydrogen spill analysis, and more.

Appendix

A. Some Raw Flame Heat Flux Data

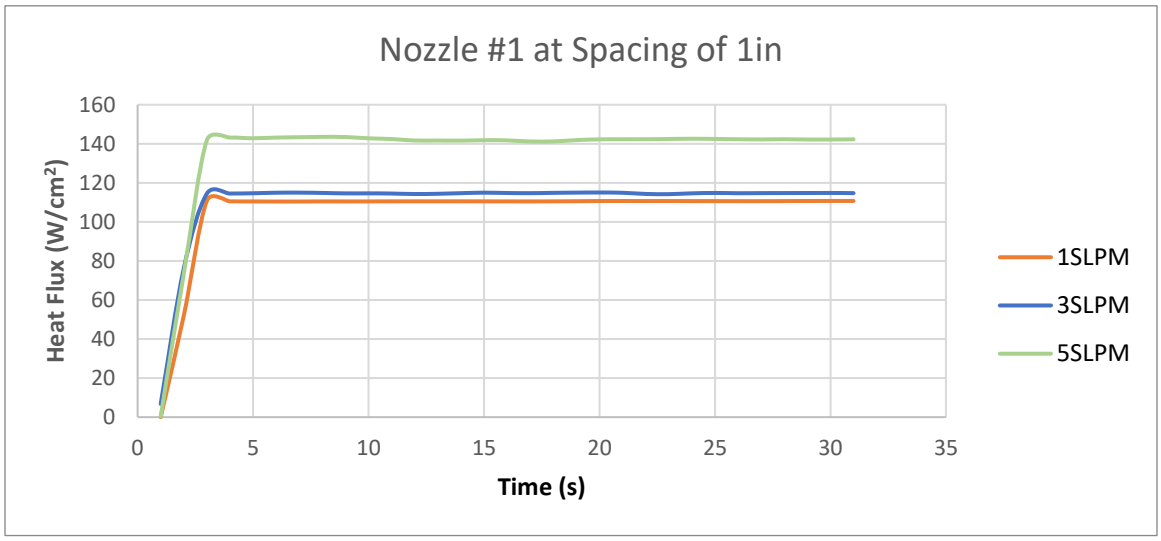

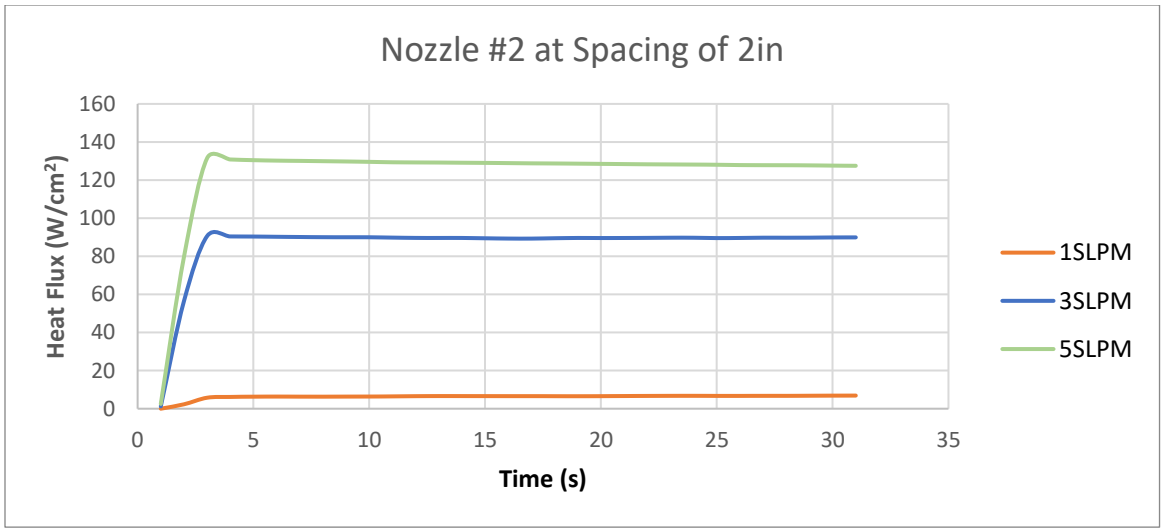

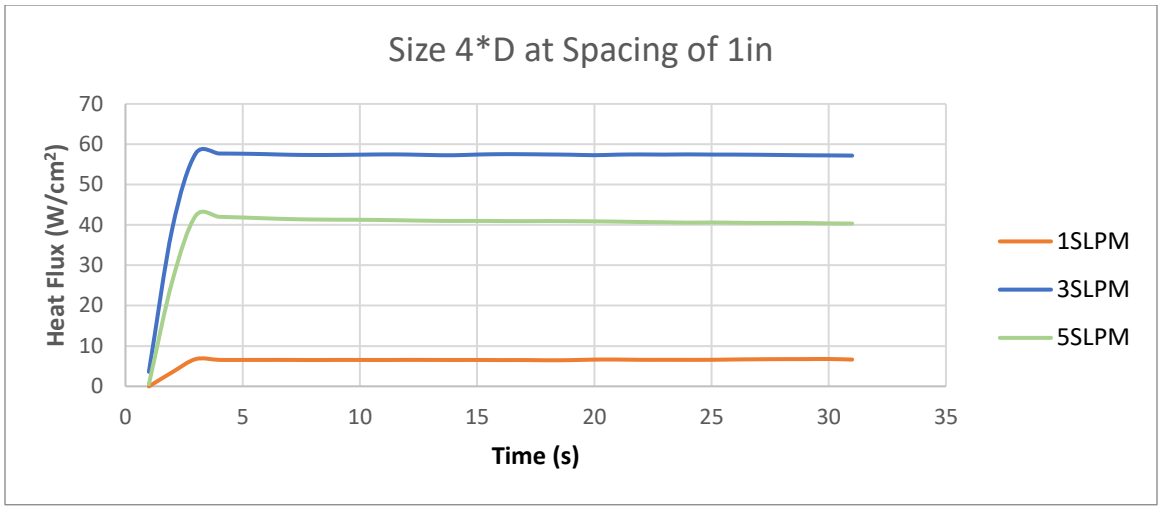
Size 4*D at Spacing of 1in
Heat Flux (W/cm²)
70
60
50
40
30
20
10
0
0
5
10
15
20
25
30
35
Time (s)
1SLPM
3SLPM
5SLPM

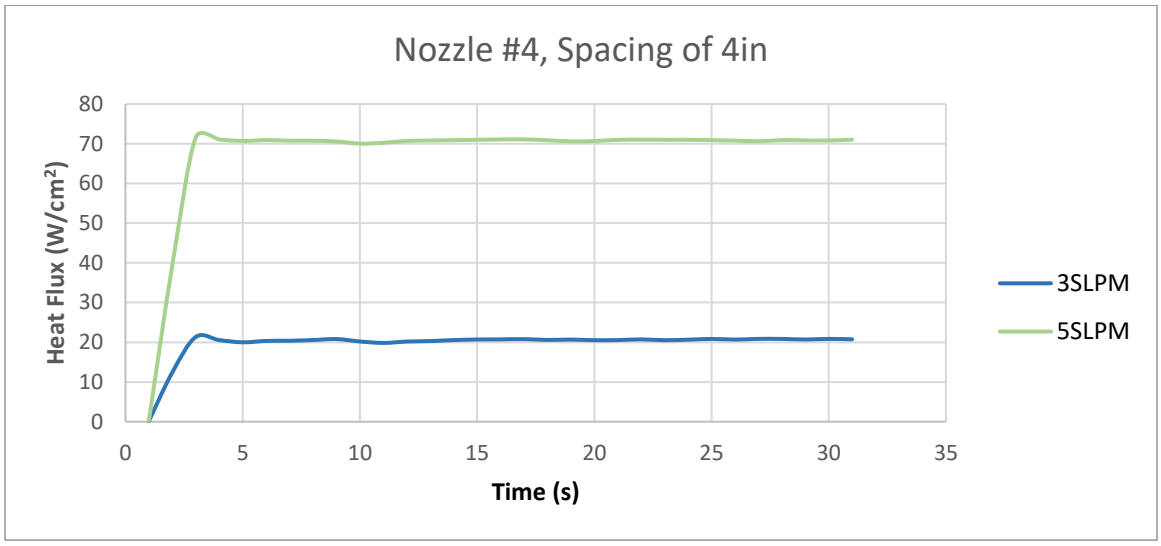
Nozzle #4, Spacing of 4in
Heat Flux (W/cm²)
80
70
60
50
40
30
20
10
0
0
5
10
15
20
25
30
35
Time (s)
3SLPM
5SLPM

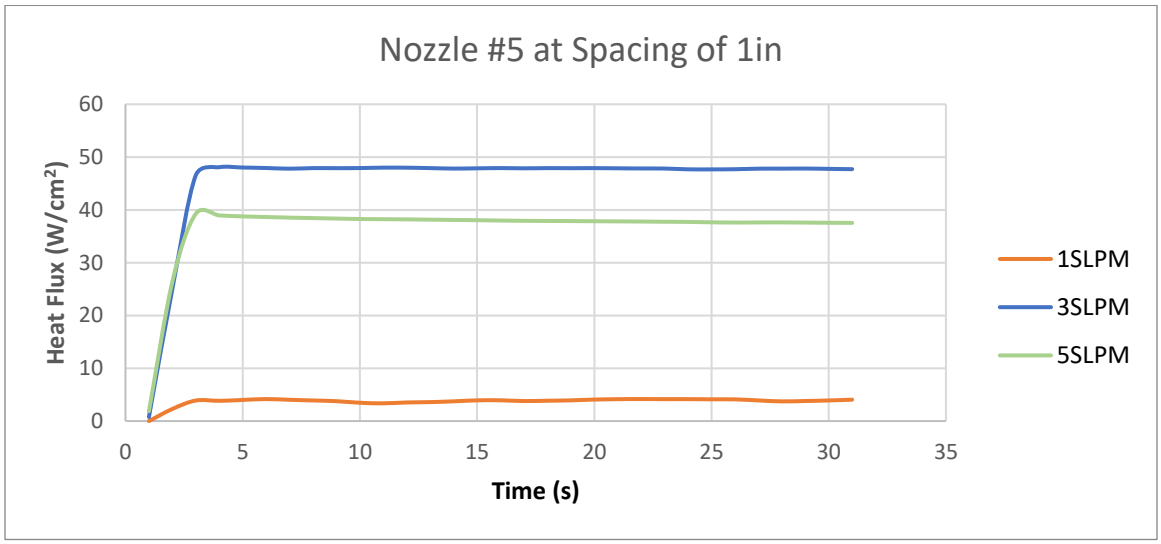
Nozzle #5 at Spacing of 1in
Heat Flux (W/cm²)
60
50
40
30
20
10
0
0
5
10
15
20
25
30
35
Time (s)
1SLPM
3SLPM
5SLPM

B. Some Raw Flame Temperature Data

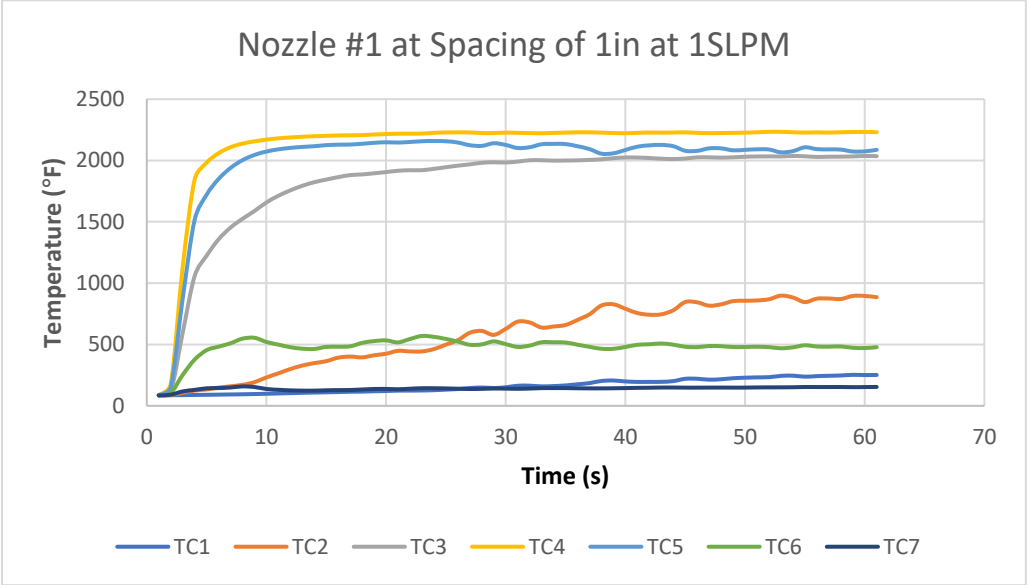

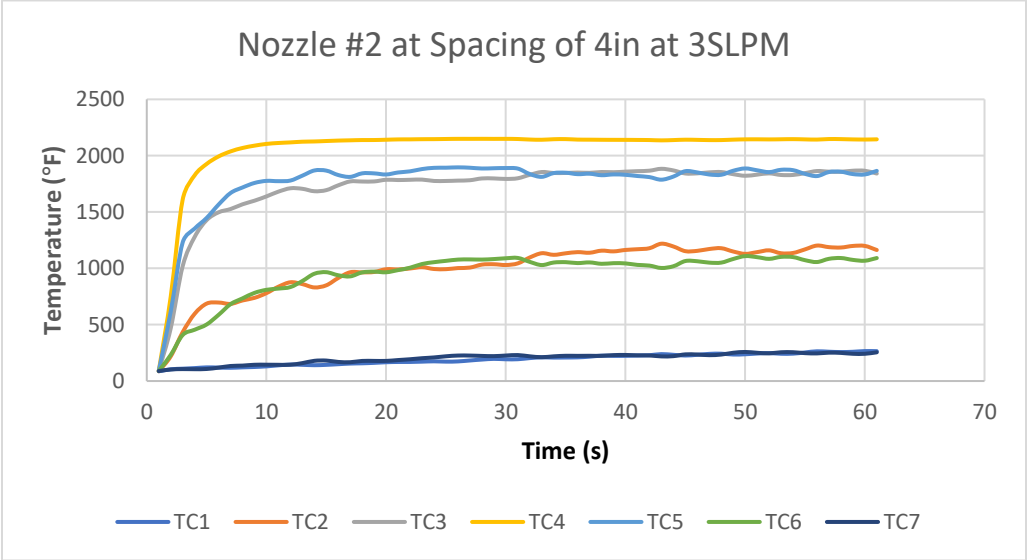

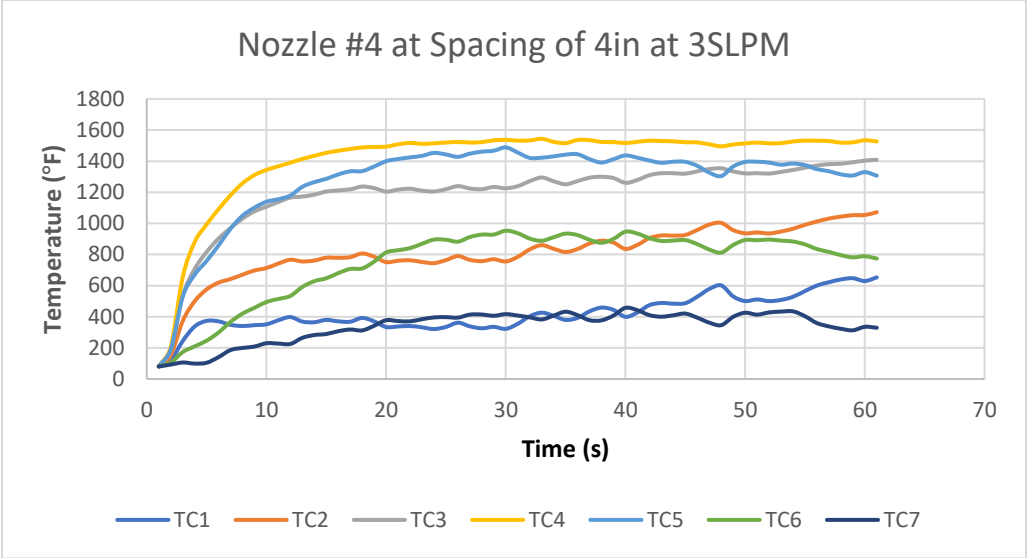
Nozzle #4 at Spacing of 4in at 3SLPM
Temperature (°F)
1800
1600
1400
1200
1000
800
600
400
200
0
0
10
20
30
40
50
60
70
Time (s)
TC1
TC2
TC3
TC4
TC5
TC6
TC7

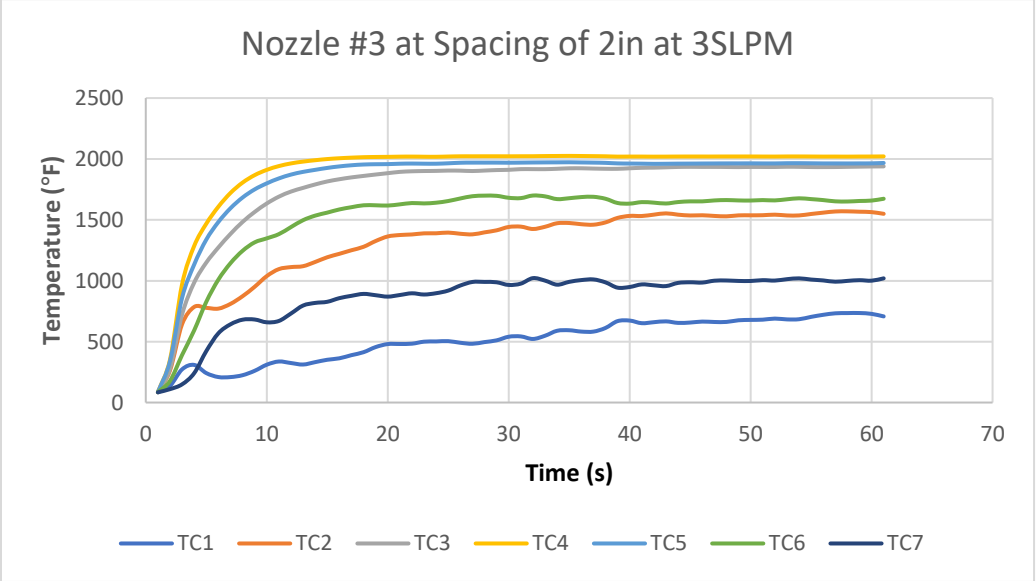
Nozzle #3 at Spacing of 2in at 3SLPM
Temperature (°F)
2500
2000
1500
1000
500
0
0
10
20
30
40
50
60
70
Time (s)
TC1
TC2
TC3
TC4
TC5
TC6
TC7

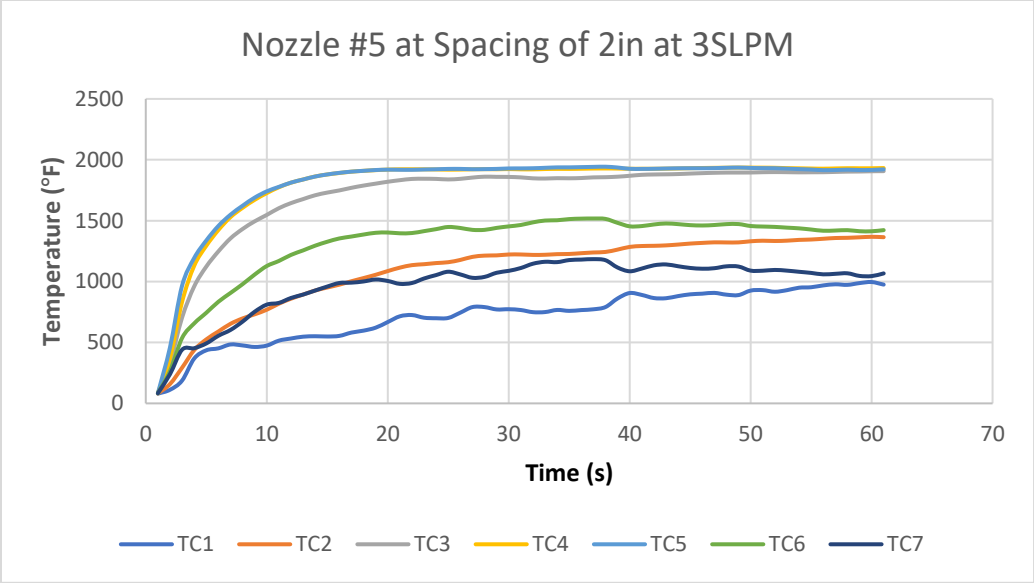
Nozzle #5 at Spacing of 2in at 3SLPM
Temperature (°F)
2500
2000
1500
1000
500
0
0
10
20
30
40
50
60
70
Time (s)
TC1
TC2
TC3
TC4
TC5
TC6
TC7

References

[1] Y. Hajji, M. Bouteraa, P. Bournot, M. Bououdina," Assessment of an accidental hydrogen leak from a vehicle tank in a confined space", International Journal of Hydrogen Energy, vol. 46(66), pp. 28710-28720, 2022.

[2] J.S. Kim, W. Yang, Y. Kim, S.H. Won, "Behavior of buoyancy and momentum controlled hydrogen jets and flames emitted into the quiescent atmosphere", Journal of Loss Prevention in the Process Industries, vol. 22, pp 943-949, 2009.

[3] E.S. Hecht, B.R. Chowdhury, "Characteristic of cryogenic hydrogen flames from high-aspect ratio nozzles", International Journal of Hydrogen Energy, vol. 46(23), pp 12320-12328, 2021.

[4] M. Henriksen, A.V. Gaathaug, J. Lundberg, "Determination of underexpanded hydrogen jet flame length with a complex nozzle geometry", International Journal of Hydrogen Energy, vol. 44(17), pp. 8988-8996, 2019.

[5] K. Zhang, T. Luo, Y. Li, T. Zhang, X. Li, Z. Zhang, S. Shang, Y. Zhou, C. Zhang, X. Chen, W. Gao, "Effect of ignition, initial pressure and temperature on the lower flammability limit of hydrogen/air mixture", International Journal of Hydrogen Energy, vol. 47(33), pp. 15107-15119, 2022.

[6] H. Kobayashi, Y. Naruo, Y. Maru, Y. Takesaki, K. Miyanabe, "Experiment of cryo-compressed (90-MPa) hydrogen leakage diffusion", International Journal of Hydrogen Energy, vol. 43(37), pp. 17928-17937, 2018.

[7] H. Kobayashi, D. Muto, Y. Daimon, Y. Umemura, Y. Takesaki, Y. Maru, T. Yagishita, S. Nonaka, K. Miyanabe, "Experimental study on cryo-compressed hydrogen ignition and flame", International Journal of Hydrogen Energy, vol. 45(7), pp. 5098-5109, 2020.

[8] T. Mogi, S. Horiguchi, "Experimental study on the hazards of high-pressure hydrogen jet diffusion flames", Journal of Loss Prevention in the Process Industries, vol. 22, pp. 45-51, 2009.

[9] Z. Wang, K. Zhou, L. Zhang, X. Nie, Y. Wu, J. Jiang, A. Simone Dederichs, L. He, "Flame extension area and temperature profile of horizontal jet fire impinging on a vertical plate", Process Safety and Environmental Protection, vol. 147, pp. 547-558, 2021.

[10] S. Chander, A. Ray, "Flame impingement heat transfer: A review", Energy Conversion and Management, vol. 46, pp. 2803-2837, 2005.

[11] L.L. Dong, C.S. Cheung, C.W. Leung, "Heat transfer characteristics of an impinging inverse diffusion flame jet. Part II: Impinging flame structure and impingement heat transfer", International Journal of Heat and Mass Transfer, vol. 50, pp. 5124-5138, 2007.

[12] C. Proust, D. Jamois, E. Studer, "High pressure hydrogen fires", International Journal of Hydrogen Energy, vol. 36, pp. 2367-2373, 2011.

[13] "Biennial Report on Hydrogen Safety", HySafe International Association For Hydrogen Safety, 2007, [Online], Available: http://www.hysafe.org/BRHS.

[14] P. P. Panda, E. S. Hecht, “Ignition and flame characteristics of cryogenic hydrogen releases”, International Journal of Hydrogen Energy, vol. 42(1), pp. 775-785, 2017.

[15] M.S. Butler, C.W. Moran, P.B. Sunderland, R.L. Axelbaum, “Limits for hydrogen leaks that can support stable flames”, International Journal of Hydrogen Energy, vol. 34, pp. 5174-5182, 2009.

[16] Z. Shu, G. Lei, Z. Liu, W. Liang, X. Zheng, J. Ma, F. Lu, H. Qian, “Motion trajectory prediction model of hydrogen leak and diffusion in a stable thermally stratified environment”, International Journal of Hydrogen Energy, vol. 47(3), pp. 2040-2049, 2022.

[17] V.V. Golub, D.I. Baklanov, T.V. Bazhenova, S.V. Golovastov, M.F. Ivanov, I.N. Laskin, N.V. Semin, V.V. Volodin, “Experimental and numerical investigation of hydrogen gas auto-ignition”, International Journal of Hydrogen Energy, vol. 34, pp. 5946-5953, 2009.

[18] A.J. Ruggles, I.W. Ekoto, “Experimental investigation of nozzle aspect ratio effects on underexpanded hydrogen jet release characteristics”, vol. 39(35), pp. 20331-20338, 2014.

[19] A. Friedrich, W. Breitung, G. Stern, A. Veser, M. Kuznetsov, G. Fast, B. Oechsler, N. Kotchourko, T. Jordan, J.R. Travis, J. Xiao, M. Schwall, M. Rottenecker, “Ignition and heat radiation of cryogenic hydrogen jets”, International Journal of Hydrogen Energy, vol. 37(22), pp. 17589-17598, 2012.

[20] J. Huete, P. Pilidis, “Parametric study on tank integration for hydrogen civil aviation propulsion”, International Journal of Hydrogen Energy, vol 46(74), pp. 37049-37062, 2021.

[21] L. Carmignani, “Flame Tracker: An image analysis program to measure flame characteristics”, SoftwareX, vol. 15, 100791, 2021.

[22] A. Lanz, J. Heffel, C. Messer, “Hydrogen Fuel Cell Engines and Related Technologies”, College of the Desert Energy Technology Training Center, 2001, [Online] Available: https://rosap.ntl.bts.gov/view/dot/14966.